ELSEVIER

Journal of South American Earth Sciences 18 (2005) 107–124

Journal of
South American
Earth Sciences

www.elsevier.com/locate/jsames

# The Late Pliocene mafic lavas from the Camusú Aike volcanic field (~50°S, Argentina): Evidence for geochemical variability in slab window magmatism

M. D'Orazio[a,b,*], F. Innocenti[a,b], P. Manetti[b], M.J. Haller[c], G. Di Vincenzo[b], S. Tonarini[b]

[a]*Dipartimento di Scienze della Terra, Università di Pisa, Via S. Maria 53, I-56126 Pisa, Italy*
[b]*Istituto di Geoscienze e Georisorse, CNR, Via Moruzzi 1, I-56124 Pisa, Italy*
[c]*Universidad Nacional de la Patagonia San Juan Bosco, CENPAT-CONICET, Puerto Madryn, Argentina*

Received 1 July 2003; accepted 1 October 2004

**Abstract**

The Camusú Aike volcanic field (CAVF), part of the discontinuous N–S-trending belt of Cenozoic mafic lava formations that occur in a backarc position along extra-Andean Patagonia, is located in southern Patagonia (~50°S, Santa Cruz province), approximately 70 km east of the extensive Meseta de las Vizcachas and just south of the upper Río Santa Cruz valley. The CAVF volcanics cover a surface of ~200 km$^2$ and occur mainly as lava flows and scoria cones. They are subdivided into two groups: Group I volcanics are high-$TiO_2$, low-Mg# olivine-hypersthene-normative basalts and trachybasalts that erupted at about 2.9 Ma; Group II lavas are much less abundant, more primitive basaltic andesites that erupted at about 2.5 Ma. Both groups show a within-plate geochemical signature, though it is more marked in Group I lavas.

The main geochemical characteristics, age, and location of CAVF volcanics are consistent with the slab window opening model proposed by different authors for the genesis of the Miocene-Recent mafic magmatism of Patagonia south of 46.5°S. The whole-rock geochemical and Sr–Nd isotope features of Group I lavas ($^{87}Sr/^{86}Sr = 0.7035–0.7037$; $^{143}Nd/^{144}Nd = 0.51288–0.51291$) indicate a genetic link between these lavas and the primitive basalts in southernmost Patagonia (Pali Aike volcanic field and Estancia Glencross area), which have been interpreted as melting products of an isotopically depleted asthenosphere. The relatively evolved compositions of the erupted Group I magmas are modeled by a polybaric crystal fractionation process without significant involvement of crustal contamination. The more primitive Group II lavas are strongly depleted in incompatible elements, have slightly higher (LREE + Ba + Th + U)/HFSE ratios, and have more enriched Sr–Nd isotope compositions ($^{87}Sr/^{86}Sr \approx 0.7039$; $^{143}Nd/^{144}Nd \approx 0.51277$) that are more akin to the Patagonian basalts farther to the north. The most likely explanation for the geochemical features of Group II lavas is the occurrence in their mantle source of a small proportion of a subduction-related, enriched component that likely resides in the former mantle wedge or the basal continental lithospheric mantle.


*Keywords:* Basaltic magmas; Geodynamics; Late Cenozoic; Patagonia; Petrology

## 1. Introduction

The voluminous effusion of basaltic plateau lavas is one the most prominent events that occurred during the Cenozoic geological history of extra-Andean Patagonia (Stern et al., 1990 and references therein). Some recent geochemistry and petrology research has focused on the origin and geodynamic significance of the Miocene-Quaternary basalts exposed in southern Patagonia, south of 46.5°S latitude (D'Orazio et al., 2000, 2001; Gorring and Kay, 2001; Gorring et al., 2003). The most accepted interpretation of this magmatism relates the production of magmas to the opening of a slab window under this sector of South America in response to the subduction of the Chile oceanic spreading ridge at the Chile Triple Junction (Ramos and Kay, 1992; Gorring et al., 1997). Although the geology of some southern Patagonia volcanic areas of this magmatic province has been studied adequately (e.g. Pali Aike volcanic field (hereafter, PAVF), Skewes and Stern, 1979; Meseta del Lago Buenos Aires, Baker et al., 1981; Estancia Glencross area (hereafter, EGA) volcanics,

* Corresponding author. Fax: +39 050 221 5800.
*E-mail address:* dorazio@dst.unipi.it (M. D'Orazio).

0895-9811/$ - see front matter © 2004 Elsevier Ltd. All rights reserved.
doi:10.1016/j.jsames.2004.10.001

D'Orazio et al., 2001), other areas, though they extend for many hundreds of square kilometers, remain almost unexplored or at a preliminary stage of investigation.

In this article, we report on the petrography, geochemistry, and geochronology of a volcanic field located south of the upper Río Santa Cruz valley and approximately 50 km east of Lago Argentino. Before this study, the extent of knowledge about the volcanic rocks in this area was extremely limited. Gathered through a field survey and sampling carried out in austral summer 2000, the collected data show that these rocks were erupted during the Late Pliocene and belong to two markedly different groups: (1) a group of lavas and scoriae consisting of moderately subalkaline basalt and trachybasalt with high-$TiO_2$ content and relatively low Mg#s and (2) a group of lavas consisting of volumetrically subordinate basaltic andesites characterized by high-$SiO_2$ and -MgO contents and low alkalis. Our study of magmas erupted in this area provides a further opportunity to characterize the nature of the Neogene-Quaternary basaltic magmatism of southern Patagonia better and understand its origin and space-time evolution.

## 2. Regional geological framework

At the latitudes of the study area, the South American continent is structured, from west to east, of four main units (Winslow, 1982; Ramos, 1988): (1) a Paleozoic metamorphic basement intruded by the Jurassic-Miocene, calc-alkaline, Patagonian batholith and exposed in the Pacific Archipelago (Hervé et al., 1981); (2) the Patagonian Cordillera, made up of deformed silicic volcanics (Late Jurassic, Tobifera or El Quemado complex) and an ophiolitic/volcaniclastic assemblage from the Early Cretaceous 'Rocas Verdes' backarc basin (Dalziel, 1981); (3) the Andean Cordillera foothills, a thin-skinned fold-and-thrust belt built up from the Late Cretaceous to the Late Miocene (Kraemer, 1998; Coutand et al., 1999); and (4) the Magallanes foreland, affected by Neogene extensional tectonics that gave rise to graben systems (Diraison et al., 1997). The latter two units consist of Jurassic-Quaternary volcano-sedimentary formations of the Magallanes basin (Biddle et al., 1986; Ramos, 1989).

The basaltic rocks of this study are located above the northern part of the Magallanes sedimentary basin, where it attains a thickness of 1000–2000 m (Biddle et al., 1986), and in proximity to the eastern margin of the Andean foothills. Kraemer et al. (1996) present an E–W regional geologic section of the Patagonian Andes and Magallanes basin at the latitude of the study area (50°20′S). On the basis of gravimetric and geologic field data, they propose that the crust under the Magallanes basin thickened during the Pliocene–Pleistocene by emplacement of mafic igneous rocks in the subsedimentary crust to its present thickness of approximately 30 km.

During the last 15 million years, the geodynamic evolution of southern South America has been largely influenced by the collision of the Chile ridge, which separates the Nazca plate from the Antarctic plate, with the Chile trench (Fig. 1). According to the plate reconstruction models of Cande and Leslie (1986), the Chile ridge started colliding with the Chile trench at the latitude of Tierra del Fuego at 14–15 Ma and formed a trench–trench–ridge triple junction. Because of plate margin configuration, the triple junction migrated northward to its present position close to the Taitao Peninsula (~46.5°S). This ridge–trench collision along the Pacific margin of southern South America is tightly linked to some prominent Cenozoic geological features, such as the formation of a volcanic gap in the modern calc-alkaline volcanic arc along the sector of the Andean Cordillera between the Chile Triple Junction and the Austral volcanic zone (Futa and Stern, 1988; Ramos and Kay, 1992; Stern and Kilian, 1996), the Neogene uplift of this sector of the Cordillera (Ramos, 1989), and the Miocene-Quaternary eruption of basaltic lavas with intraplate geochemical affinity in a backarc position (Ramos and Kay, 1992; Gorring et al., 1997; D'Orazio et al., 2000, 2001). Recently, modeling of isostatic rebound related to advances and retreats of the Patagonian ice fields (Ivins and James, 1999) has indicated an anomalously low viscosity mantle and thin lithosphere, compatible with a slab window that formed in response to the ridge-trench collision under this sector of South America.

## 3. The Camusú Aike volcanic field

We assign the volcanic field in this study the name Camusú Aike volcanic field (CAVF, hereafter), after the name of a stream crossing this area; in the ancient Tehuelche language, the word Camusù refers to the wavy, flame-like movement of the grass. The CAVF is located between 50°17′S and 50°34′S and between 71°00′W and 71°19′W, covers a surface of ~200 $km^2$ (Fig. 2), and is composed of a sequence of lava flows that issue from several scoria cones and eruptive fissures. These volcanic rocks lie atop the Meseta Pampa Alta, a widespread high plain located south of the upper Río Santa Cruz valley that slopes to the southeast with a ~1% gradient. According to Strelin et al. (1999), this meseta is a proglacial plain emerging east of the moraine deposits of the Pampa Alta glaciation, 10 km west of the CAVF. Within the study area, the Meseta Pampa Alta attains elevations of 700–420 m above sea level (a.s.l.) and is crossed by several flat-bottomed stream valleys (e.g. Cañadón Camusú Aike, Cañadón Deus; Fig. 2). The proglacial deposits of the Meseta Pampa Alta are gravels with clasts of schists, acidic volcanics, and granitoid rocks, sometimes intercalated with sandy lenses.

The volcanic cones of the CAVF are distributed along an ENE–WSW band in the northern sector of

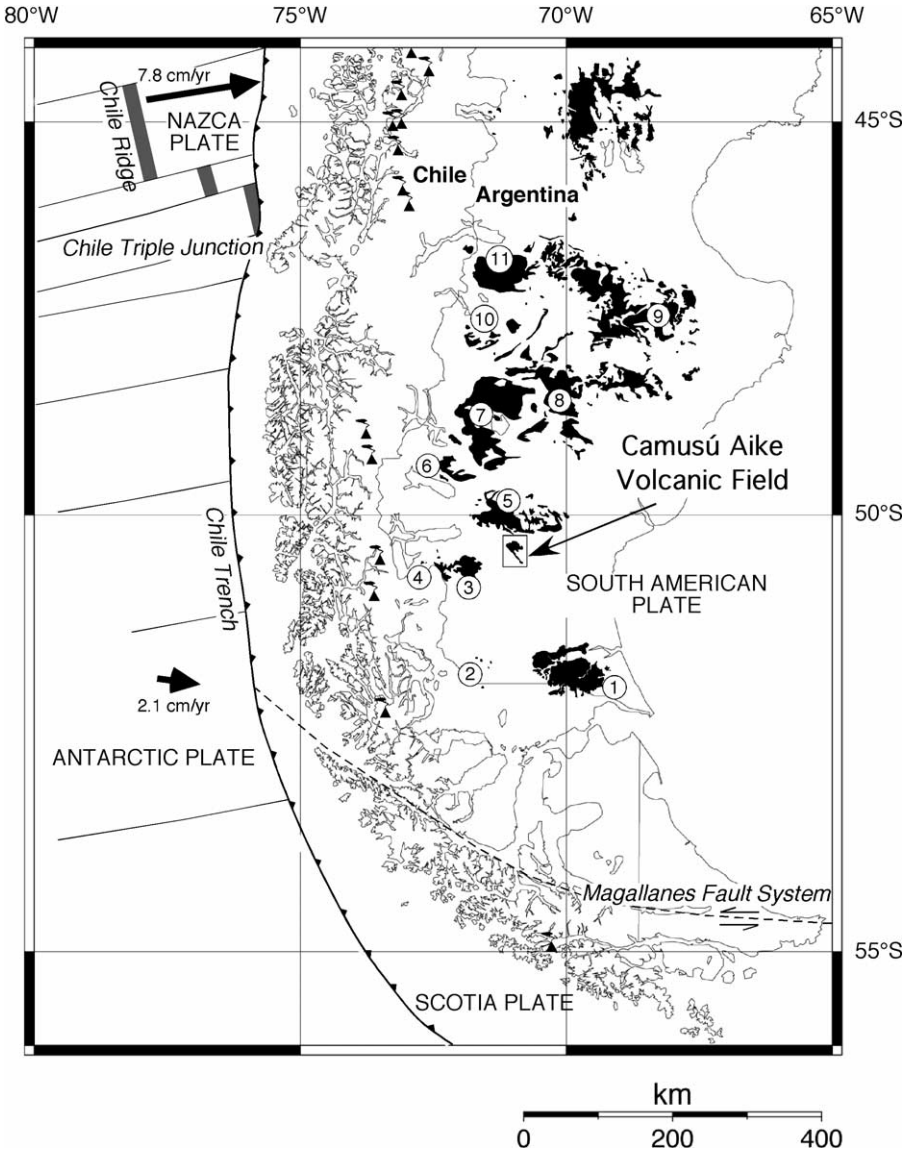


Fig. 1. Schematic geodynamic setting of southern South America and adjacent Pacific Ocean. The sketch shows the fracture zones of the oceanic Nazca and Antarctic plates (thin continuous lines), the Chile oceanic spreading ridge (grey strips), the Chile trench (heavy continuous line with triangles on the overriding plate), the transcurrent margin between the Scotia and South American plates (dashed line), the Chile Triple Junction, the main active volcanoes of the Andean Cordillera (filled smoking triangles), and the Cenozoic Patagonian lavas (black areas). The two large, black arrows are the convergence vectors of the Nazca and Antarctic plates with respect to South America, according to the NUVEL-1A model of DeMets et al. (1994). The boxed area shows the studied zone (enlarged in Fig. 2). Circled numbers are Patagonian basalt occurrences cited in the text: 1. Pali Aike volcanic field (Late Pliocene-Quaternary); 2. Estancia Glencross area (Late Miocene); 3. Meseta de las Vizcachas (Middle Miocene–Late Pliocene); 4. Cerro del Fraile (Late Pliocene-Quaternary); 5. mesetas north of Río Santa Cruz valley (Miocene?–Late Pliocene); 6. Meseta del Viento (Early Pliocene–Late Pliocene); 7. Meseta de la Muerte and Meseta Strobel (Middle Miocene–Early Pliocene); 8. Meseta Central (Late Miocene–Late Pliocene); 9. mesetas north and northeast of the Deseado Massif (Eocene–Late Pliocene); 10. Meseta Belgrano (Late Miocene–Late Pliocene); and 11. Meseta del Lago Buenos Aires (Paleocene-Quaternary).

the volcanic field (Fig. 2). Through field surveys and satellite image analysis, we recognize six main scoria cones (basal diameter 1000–2000 m) and several minor scoria cones and scoria ramparts. The largest scoria cone, the Cerro Grande (767 m a.s.l.), rises approximately 120 m above the surrounding plain. Another, located at 50°20′S, 71°14′W (752 m a.s.l.), is characterized by a large breaching to the west (Fig. 3a). The cones are made up of red to black scoriae, sometimes with large ellipsoidal bombs (up to 45 cm maximum length), and subordinate spattered material.

One of the most prominent volcanic features of the CAVF is an elongated structure consisting of several long, piled lava flows. These flows start at the NW corner of the volcanic field, close to the base of the cone at 50°20′S, 71°14′W; the longest one ends 33 km to the SE near Estancia La Paz (Figs. 2 and 3b). Other lava flows that form the CAVF occur as flat pahoehoe sheets.

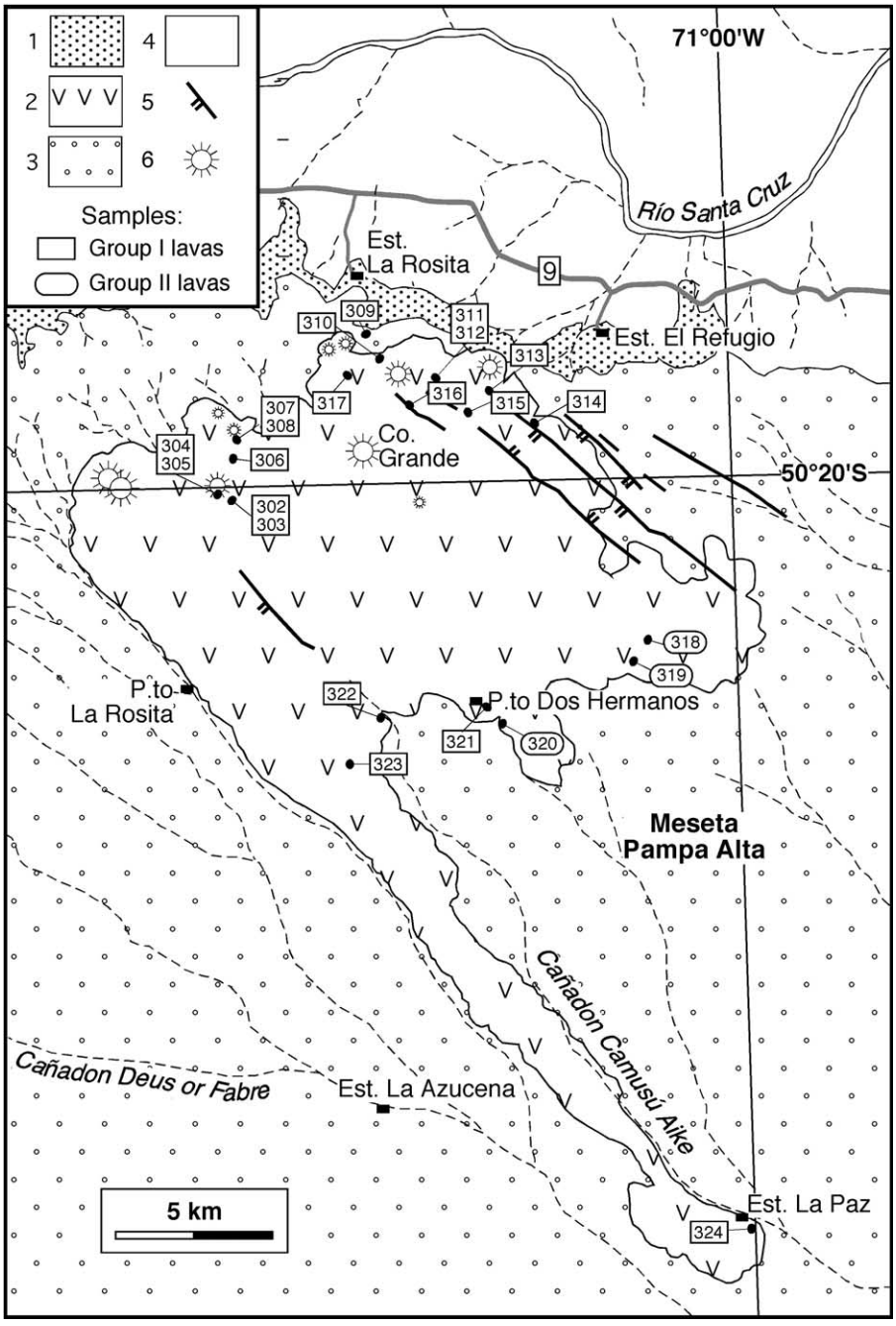


Fig. 2. Geological sketch map of the CAVF. Legend: 1. Santa Cruz Formation (Middle Miocene); 2. Camusú Aike volcanics (Upper Pliocene); 3. Meseta Pampa Alta fluvioglacial deposits (Upper Pliocene-Quaternary); 4. alluvial and colluvial deposits (Quaternary); 5. faults; and 6. scoria cones. The track of the Ruta Provincial 9 is also shown.

The stratigraphically lowermost lava flow found during our survey is exposed in the northern sector of the CAVF in the escarpment of the Río Santa Cruz valley, covered by a layer of fluvioglacial gravel (Fig. 3c). Discontinuous outcrops of lava flows showing irregular columnar jointing occur in the eastern sector of the CAVF and in the area around Puesto Dos Hermanos (Fig. 2).

The study area was affected by extensional tectonics, which generated a NW–SE-trending, ~10 km long, ~2.5 km wide graben structure in the northeast sector of the CAVF (Fig. 2). Marked NW–SE structural control on the volcanic activity is evidenced by the alignment of the two eroded craters and the marked channelling of the major lava flows in a NW–SE-trending morphological depression.

## 4. Analytical methods

Mineral analyses were performed at the Istituto di Geoscienze e Georisorse (CNR, Firenze) using a JEOL

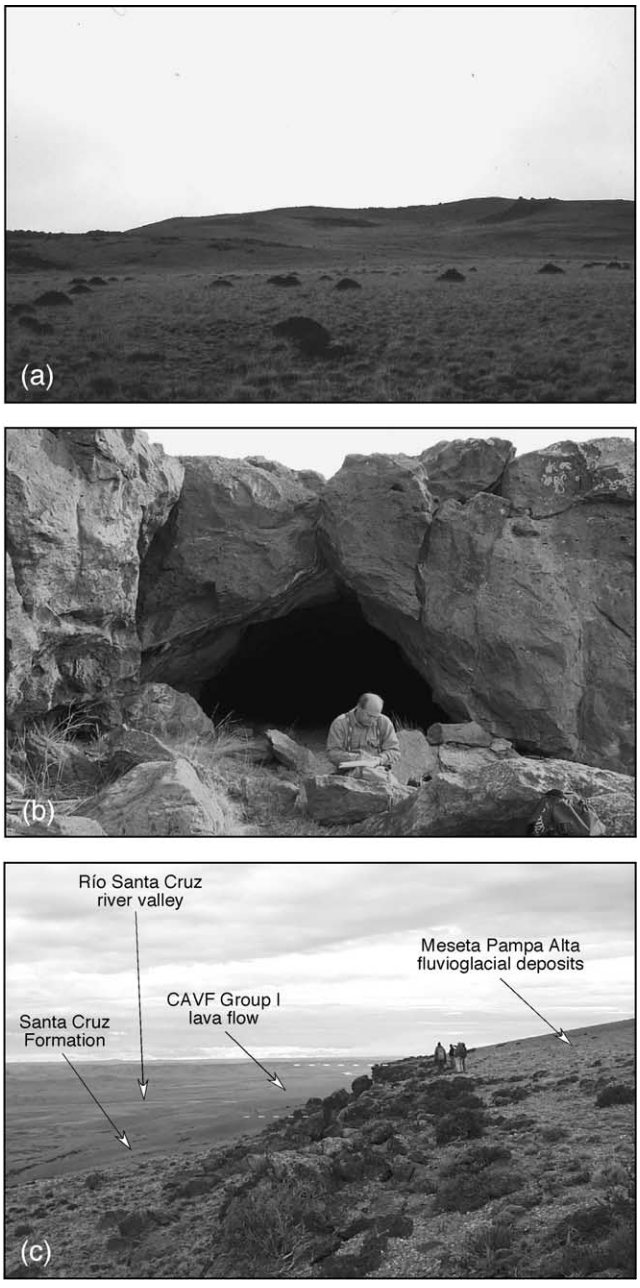


Fig. 3. (a) Eroded scoria cone (50°20′S, 71°14′W, 752 m a.s.l.) showing a wide breaching to the west, (b) lava tunnel in the basaltic flow at Estancia La Paz (sample PA-324), and (c) lava flow (sample PA-309) exposed along the uppermost flank of the Río Santa Cruz valley at the northernmost end of the CAVF. The flow, dated by $^{40}Ar$–$^{39}Ar$ at 2.95 ± 0.06 Ma, is overlain by fluvioglacial gravel.

JXA-8600 electron microprobe coupled with four WDS spectrometers. Instrumental conditions were as follows: 15 kV accelerating potential, 10 nA cup current, and 2 μm beam spot; calibration standards were natural silicates; matrix effects were corrected following Bence and Albee (1968). $SiO_2$, $TiO_2$, $Al_2O_3$, $Fe_2O_3$tot, MnO, MgO, CaO, $Na_2O$, $K_2O$, and $P_2O_5$ for the whole rocks were determined by X-ray fluorescence (ARL 9400 $XP^+$) using $Li_2B_4O_7$ glass disks (sample:flux ratio = 1:7) at the Dipartimento di Scienze della Terra, University of Pisa. FeO was determined by titration. Loss on ignition was determined by gravimetry at 1000 °C after preheating at 110 °C. The estimated precision for major element data in the concentration ranges of the studied samples is better than 2%.

The concentrations of 30 trace elements were determined by ICP-MS (VG PQII Plus STE) at the Dipartimento di Scienze della Terra, University of Pisa. Samples were dissolved in PFA vessels on a hot plate at approximately 120 °C with $HF + HNO_3$. The sample solutions, at ca. 1:1000 dilution, were measured in replicates by external calibration. Analytical precisions, evaluated by repeated analyses of the in-house standard HE-1 (Mt. Etna hawaiite), are between 2 and 5% relative standard deviation, except for Gd and Tm (6%) and Be, Sc, and Pb (8%).

Sr and Nd isotopic analyses were carried out using a Finnigan MAT 262V multicollector mass spectrometer at the Istituto di Geoscienze e Georisorse (CNR, Pisa) and conventional ion exchange methods for Sr and Nd separations. Measured $^{87}Sr/^{86}Sr$ ratios were normalized to $^{86}Sr/^{88}Sr = 0.1194$; $^{143}Nd/^{144}Nd$ ratios were normalized to $^{146}Nd/^{144}Nd = 0.7219$. During the collection of isotopic data for this study, replicate measurements of NIST SRM 987 ($SrCO_3$) and La Jolla standards gave values of 0.710240 ± 11 (2 s.d.) for $^{87}Sr/^{86}Sr$ and 0.511848 ± 26 (2 s.d.) for $^{143}Nd/^{144}Nd$.

The groundmass of samples PA-309, 320, and 324, selected for $^{40}Ar$–$^{39}Ar$ analyses (carried out at the Istituto di Geoscienze e Georisorse, CNR, Pisa), was separated by standard separation techniques and purified by hand-picking under a stereomicroscope. The separated material was further cleaned by acid leaching in an ultrasonic bath (1 h at ~50 °C in 3.5N HCl and 1N $HNO_3$). The final product was wrapped in aluminum foil and irradiated for 4 h in the TRIGA reactor (University of Pavia, Italy), along with the dating standard FCT-3 biotite (27.95 Ma; Baksi et al., 1996). After irradiation, the samples (~15–20 mg) were loaded into 8 mm diameter holes of a copper holder, placed into an ultrahigh-vacuum laser port, and baked overnight at ~180 °C. Incremental laser step-heating experiments were carried out using an infrared laser beam generated by a diode-pumped CW Nd-YAG laser, which was defocused to a ~2 mm spot. The laser beam was homogenized by a beam homogenizer lens, which produces a flat power distribution. Homogenous heating was obtained by slowly rastering the laser beam by a computer-controlled *x*–*y* stage. The steps were carried out with increasing laser powers until complete melting occurred. The gas extracted was gettered and, after 20 min (including ~6 min lasering), equilibrated by automated valves into a MAP215–50 noble gas mass spectrometer fitted with a Balzers SEV 217 secondary electron multiplier. Reported data (Table 1, Appendix A) were corrected for post-irradiation decay, mass discrimination effects, isotopes derived from interfering neutron reactions, and blanks. Errors are $2\sigma$ and do not include

Table 1
Summary of incremental $^{40}Ar$–$^{39}Ar$ step-heating data for CAVF lavas

| Sample | Size (mm) | Analyzed mass (mg) | Total fusion age ±2σ (Ma) | Ca/K ±2σ | No. step plateau | $^{39}Ar_{(K)}$ % plateau | Isochron age (Ma) | MSWD | $(^{40}Ar/^{36}Ar)_i$ | Plateau age ± 2σ (Ma) |
|---|---|---|---|---|---|---|---|---|---|---|
| PA-309 | 0.25–0.30 | 16.1 | 2.83±0.11 | 5.75±0.31 | 9 | 100 | 3.02±0.07 | 0.59 | 291±3 | 2.95±0.06 |
| PA-320 | 0.25–0.30 | 23.0 | 2.52±0.09 | 12.44±0.68 | 9 | 100 | 2.44±0.21 | 1.1 | 298±8 | 2.51±0.08 |
| PA-324 | 0.25–0.30 | 16.6 | 2.82±0.05 | 5.49±0.30 | 5 | 74.9 | 2.94±0.08 | 0.21 | 291±9 | 2.91±0.05 |

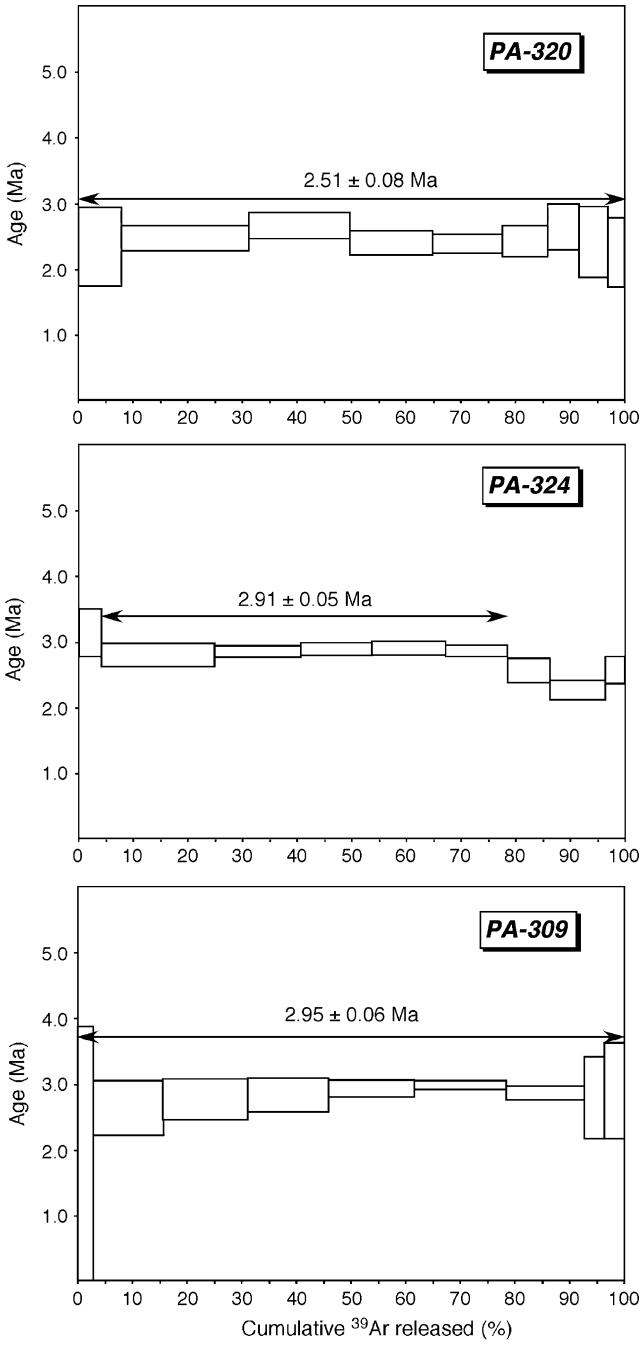


Fig. 4. Age spectra for the $^{40}Ar$–$^{39}Ar$ incremental heating analyses of samples PA-320, PA-324, and PA-309. The double-arrow segments indicate the steps used for the plateau age determination.

the uncertainty in the *J* value, which was included in the calculated plateau and total fusion ages.

## 5. $^{40}Ar$–$^{39}Ar$ geochronology

Sample PA-309 is from the lowermost, ~3 m thick lava flow exposed in the northernmost sector of the lava field on the upper flank of the Río Santa Cruz valley (660 m a.s.l.).

Sample PA-324 is from a 4 m thick lava flow at the southeastern termination of the NW–SE-elongated lava field near Estancia La Paz (440 m a.s.l.). Sample PA-320 represents a lava flow that crops out close to Puesto Dos Hermanos (550 m a.s.l.). The $^{40}Ar$–$^{39}Ar$ data are summarized in Table 1, and the age spectra for the three samples are reported in Fig. 4. All the samples analyzed yield well-defined plateaus (more than three contiguous steps that together comprise more than 50% of the $^{39}Ar_{(K)}$ released and overlap at $2\sigma$ analytical error), which we consider meaningful. The data obtained indicate that the CAVF was active during the Late Pliocene for at least 450 ka. Recently, Mejia et al. (2004) published a paleomagnetic study of the Plio-Pleistocene mafic lavas of southern Patagonia in which they report two $^{40}Ar$–$^{39}Ar$ dates of lavas from the CAVF of $2.98 \pm 0.03$ Ma and $3.02 \pm 0.04$ Ma, in close agreement with our data. The $^{40}Ar$–$^{39}Ar$ age determinations from our work and Mejia et al. (2004) contrast with a single $^{40}Ar$–$^{39}Ar$ age of $0.67 \pm 0.56$ Ma quoted by Strelin et al. (1999) for a lava flow from the central portion of the NW–SE-elongated lava field. Unfortunately, the possible cause of the mismatch between these data cannot be evaluated because of the lack of the analytical details for the latter $^{40}Ar$–$^{39}Ar$ determination.

## 6. Classification and petrography

As we show in the total alkali versus silica classification diagram (Fig. 5), the majority of the volcanic rocks exposed in the CAVF are hypersthene + olivine-normative basalts and trachybasalts (hawaiites) (Group I; Fig. 5), whereas the rare lavas with columnar jointing sampled in the Puesto Dos Hermanos area are quartz-normative basaltic andesites (Group II; Fig. 5).

Basalt and trachybasalt rocks have textures that vary between two extreme petrographic types. Most trachybasalts (e.g. PA-303, 305, 306) are aphyric or subaphyric with rare phenocrysts of corroded plagioclase and Ti-magnetite microphenocrysts. They can be vesiculated or massive and have a microcrystalline groundmass of plagioclase microlites, clinopyroxene, Fe–Ti oxides, and olivine. The other petrographic type includes porphyritic rocks (mostly basalts; e.g. PA-314, 315) with phenocrysts of plagioclase, olivine, and Fe–Ti oxides. These rocks have a total phenocryst content of approximately 20 vol.% and are characterized by plagioclase megacrysts up to 2–3 cm maximum length. Typically, these megacrysts are devoid of inclusions and, in some cases, appear strongly resorbed. In the latter case, they show a calcic plagioclase rim ($An_{67}$) around a homogeneous, more sodic ($An_{54}$) core (Fig. 6). Olivine microphenocrysts are zoned with $Fo_{68–71}$ cores and $Fo_{53–57}$ rims (Fig. 6). The groundmass consists of plagioclase ($An_{52–59}$), subophitic clinopyroxene ($Wo_{40–43}En_{37–38}$), olivine ($Fo_{52–64}$),

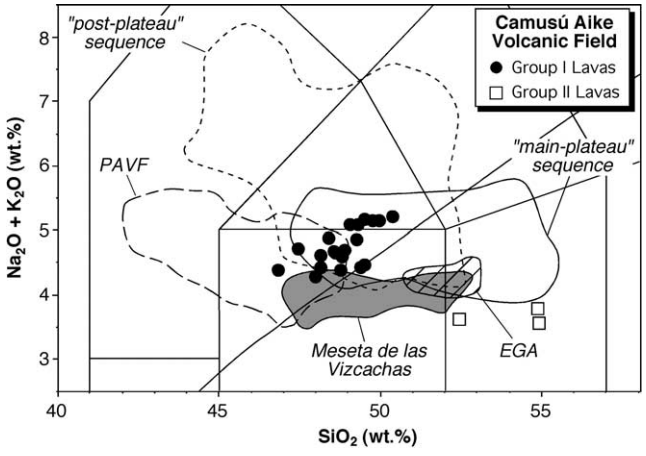


Fig. 5. Total alkalis versus silica (wt.%) diagram for the studied rocks. The fields for the volcanics from the PAVF (D'Orazio et al., 2000), EGA (D'Orazio et al., 2001), Meseta de las Vizcachas (authors' unpublished data), and the main- and postplateau sequences of southern Patagonia (MgO > 6 wt.%; Gorring, 1997) are shown for comparison. The boundary line between alkaline and subalkaline rocks is also plotted (Irvine and Baragar, 1971).

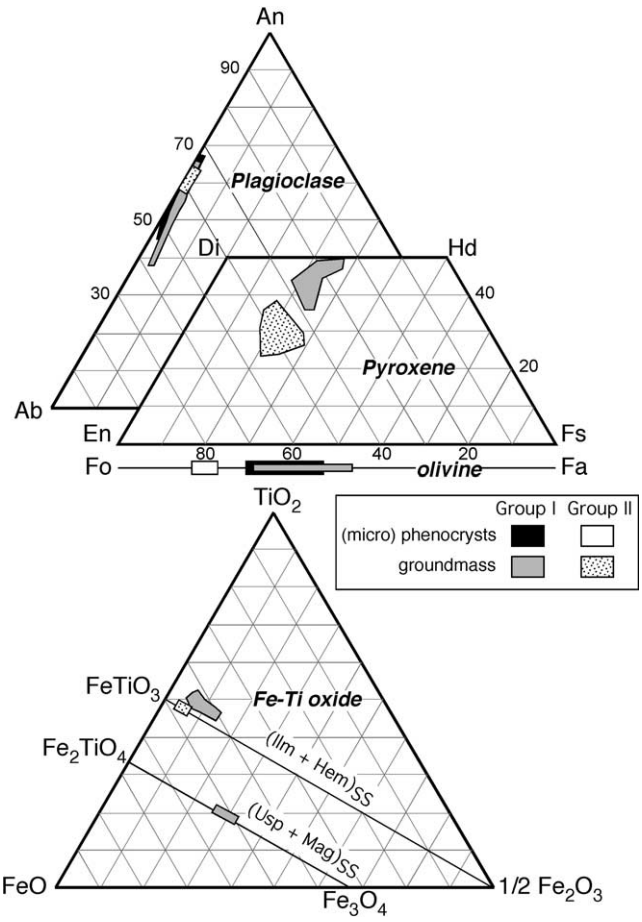


Fig. 6. Compositions of plagioclases, clinopyroxenes, olivines, and Fe–Ti oxides from the CAVF plotted in an Ab–An–Or triangle, Di–Hd–En–Fs quadrilateral, Fo–Fa join, and FeO–$TiO_2$-1/2$Fe_2O_3$ triangle, respectively.

ilmenite, and Ti-magnetite. Lavas with textures between the two extreme petrographic types are moderately porphyritic with phenocrysts of plagioclase (cores $An_{53–58}$, rims $An_{54–67}$) and microphenocrysts of olivine (cores $Fo_{62–64}$, rims $Fo_{55–57}$) and Fe–Ti oxides. The groundmass is composed of labradorite microlites, diopside ($Wo_{37–48}En_{26–38}$), olivine ($Fo_{37–69}$), ilmenite, and Ti-magnetite. The ilmenite crystals of the Group I lavas are characterized by an elevated content of the geikielite component, which causes the data points to plot above the ilmenite–hematite tie line in the Fe–Ti oxide compositional triangle in Fig. 6.

Basaltic andesite rocks are olivine-phyric rocks containing ~5 vol.% of olivine phenocrysts with forsteritic cores ($Fo_{79–82}$) and less magnesian rims ($Fo_{64}$) (Fig. 6). The groundmass is composed of labradorite ($An_{58–63}$) microlites, augite ($Wo_{26–31}En_{44–53}$), and abundant ilmenite as the unique Fe–Ti oxide phase. The groundmass pyroxene of these lavas is distinctly less enriched in the Wo component than are the Group I lavas (Fig. 6).

The coexistence of titanomagnetite and ilmenite in the groundmass of the PA-324 lava (Estancia La Paz) enables us to estimate the temperature and $fO_2$ of equilibration. By applying Ghiorso and Sack (1991) geothermometer to the average compositions of the two coexisting Fe–Ti oxide phases, we find an equilibrium temperature of 1080 °C and oxygen fugacities of $10^{-9.3}$ atm (+0.6 ΔFMQ log units). Sample PA-302 contains skeletal Ti-magnetite microphenocrysts with exsolution lamellae of ilmenite. By applying Ghiorso and Sack (1991) geothermometer to these coexisting Fe–Ti oxides, we obtain a temperature of 805 °C, probably close to the subsolidus reequilibration temperature of the Fe–Ti oxide minerals in this rock.

## 7. Geochemistry and Sr–Nd isotopes

We report major- and trace-element analyses of representative samples from the CAVF in Table 2. On the basis of the whole-rock chemistry, we confirm the distinction of the two different group of rocks from the CAVF. Group I basalts and trachybasalts have relatively low MgO and $K_2O$ contents (4.2–5.1 wt.% and 0.8–1.5 wt.%, respectively), low Mg#s (42–49), and high $TiO_2$ (3.0–4.2 wt.%). Group II basaltic andesite lavas have higher MgO (6.6–7.2 wt.%) and Mg#s (~60) and lower $TiO_2$ and $K_2O$ (1.9–2.0 wt.% and 0.4–0.6 wt.%, respectively). The low MgO contents of Group I lavas are not commonly observed in the southern Patagonia Miocene-Quaternary volcanics, which usually have MgO concentrations >6 wt.% (Stern et al., 1990; D'Orazio et al., 2000, 2001; Gorring and Kay, 2001). The whole-rock chemistry of the Group II lavas is also remarkable, because mafic volcanics with high silica (>52 wt.%) and low total alkali ($Na_2O+K_2O<4$ wt%) are extremely rare in southern Patagonia (Fig. 5).

Group I lavas and scoriae have a reduced variability for most major elements except $P_2O_5$, $K_2O$, and $TiO_2$. In Fig. 7, we use the $P_2O_5$ concentration as an index of variation. With the largest variability of the data set, $P_2O_5$ shows incompatible behavior, as suggested by its good positive correlation with highly incompatible trace elements, such as Th or Ba, and the absence of optically resolvable apatite crystals in the rocks. The most remarkable major-element variations in these lavas are represented by the progressive decrease of $TiO_2$, MgO, and CaO and the increase of $K_2O$ and $Na_2O$ from the less evolved (lower $P_2O_5$) to the most evolved (higher $P_2O_5$) rocks (Fig. 7). The remaining major elements ($SiO_2$, $Al_2O_3$, and $FeO_{tot}$) show much more scattered variations.

The distribution of Cr and Ni in the CAVF lavas conforms to their MgO content. Trachybasalts of Group I are much more depleted in these elements with respect to the basalts of Group I, whereas Group II lavas show significant relative enrichments.

The incompatible element distribution of the CAVF volcanics is typical of within-plate magmas from continental and oceanic settings (e.g. Sun and McDonough, 1989). The primordial mantle-normalized trace-element patterns (Fig. 8) exhibit humped distributions with high Nb, Ta, and light rare earth elements (LREE) and relatively low large ion lithophile element (LILE) and heavy rare earth element (HREE) normalized concentrations. Among the Group I lavas, a clear difference can be observed between trachybasalts and basalts. The former are characterized by negative spikes of Sr and Ti (Fig. 8a), whereas the latter have slightly positive spikes for these elements (Fig. 8b). Group II lavas are distinguished from Group I by their lower contents of incompatible elements and lower concentrations of Nb and Ta relative to LREE and other highly incompatible elements (e.g. Ba, Th, U; Fig. 8c).

The distribution of the REE for all samples of Group I is remarkably similar; chondrite-normalized REE patterns (not shown; normalizing values after McDonough and Sun, 1995) are almost rectilinear and LREE enriched ($La_N=101–177$, $Yb_N=10.5–19.7$, $[La/Yb]_N=8.2–9.6$). Group II lavas have lower total REE contents and lower LREE/HREE ratios ($La_N=57–60$, $Yb_N=8.5–8.7$, $[La/Yb]_N=6.6–6.9$).

We determined five Sr–Nd isotope compositions for the CAVF volcanics (Table 2). $^{87}Sr/^{86}Sr$ ratios range from 0.70352 to 0.70392, and $^{143}Nd/^{144}Nd$ ratios range from 0.51291 to 0.51277. In Fig. 9, in which we have plotted the available Sr–Nd isotope compositions for the Neogene-Quaternary mafic lavas from southern Patagonia, the two Group I basaltic lavas from the CAVF, plus the plagioclase megacrysts separated from one of these lavas (PA-324), fall within the low-$^{87}Sr/^{86}Sr$, high-$^{143}Nd/^{144}Nd$ field 'A' defined by the southernmost Patagonia basalts from the PAVF and EGA. The limited number of southern Patagonia samples belonging to this group have $^{87}Sr/^{86}Sr<0.7038$ and $^{143}Nd/^{144}Nd>0.5128$. The two Group II samples are

Table 2
Chemical and Sr–Nd isotope data for selected volcanic rocks from CAVF

| | Group I volcanics | | | | | | | | | | | | Group II volcanics | | |
|---|---|---|---|---|---|---|---|---|---|---|---|---|---|---|---|
| Sample | PA-322 | PA-315 | PA-324 | PA-311 | PA-317 | PA-309 | PA-308 | PA-312 | PA-306 | PA-302 | PA-303 | PA-307 | PA-320 | PA-318 | PA-319 |
| Lat. S | 50°24′20″ | 50°19′03″ | 50°32′57″ | 50°18′06″ | 50°18′00″ | 50°17′36″ | 50°19′17″ | 50°18′05″ | 50°19′38″ | 50°20′47″ | 50°20′47″ | 50°19′22″ | 50°24′30″ | 50°23′18″ | 50°23′37″ |
| Long. W | 71°09′41″ | 71°07′33″ | 71°00′26″ | 71°08′00″ | 71°10′29″ | 71°09′37″ | 71°13′07″ | 71°07′50″ | 71°13′22″ | 71°13′20″ | 71°13′20″ | 71°13′16″ | 71°06′35″ | 71°02′22″ | 71°03′03″ |
| Rock | B | B | B | B | B | B | B | B | TB | TB | TB | TB | BA | BA | BA |
| *Major elements (wt.%)* | | | | | | | | | | | | | | | |
| $SiO_2$ | 48.11 | 47.17 | 47.25 | 46.51 | 48.59 | 47.47 | 45.85 | 48.35 | 48.47 | 50.28 | 48.70 | 48.98 | 51.56 | 55.24 | 54.32 |
| $TiO_2$ | 4.16 | 4.08 | 4.21 | 3.72 | 3.97 | 4.08 | 3.78 | 3.57 | 3.11 | 3.01 | 3.03 | 2.79 | 2.03 | 1.92 | 1.86 |
| $Al_2O_3$ | 16.38 | 15.90 | 16.84 | 16.31 | 15.53 | 15.71 | 15.56 | 15.54 | 15.98 | 16.16 | 15.85 | 17.12 | 14.63 | 14.42 | 14.24 |
| $Fe_2O_3$ | 2.90 | 2.59 | 2.60 | 3.70 | 2.71 | 8.41 | 11.42 | 3.59 | 3.40 | 2.96 | 4.17 | 3.59 | 1.47 | 1.49 | 2.08 |
| FeO | 8.79 | 10.17 | 9.08 | 9.72 | 9.61 | 4.95 | 3.11 | 8.97 | 9.55 | 9.67 | 8.59 | 8.66 | 8.85 | 8.22 | 7.62 |
| MnO | 0.13 | 0.15 | 0.14 | 0.17 | 0.16 | 0.15 | 0.17 | 0.16 | 0.18 | 0.18 | 0.18 | 0.18 | 0.14 | 0.13 | 0.13 |
| MgO | 5.13 | 5.09 | 5.01 | 4.87 | 4.85 | 4.80 | 4.75 | 4.71 | 4.30 | 4.22 | 4.18 | 4.38 | 7.17 | 6.88 | 6.64 |
| CaO | 8.08 | 8.41 | 8.09 | 7.92 | 7.92 | 8.21 | 8.47 | 7.95 | 7.60 | 7.45 | 7.49 | 7.11 | 8.71 | 8.40 | 8.30 |
| $Na_2O$ | 3.52 | 3.40 | 3.44 | 3.44 | 3.35 | 3.40 | 3.22 | 3.48 | 3.63 | 3.70 | 3.59 | 3.67 | 3.21 | 3.17 | 3.05 |
| $K_2O$ | 1.01 | 0.81 | 1.10 | 1.18 | 1.04 | 0.96 | 1.08 | 1.29 | 1.37 | 1.49 | 1.45 | 1.45 | 0.35 | 0.64 | 0.46 |
| $P_2O_5$ | 0.46 | 0.56 | 0.45 | 0.59 | 0.51 | 0.51 | 0.59 | 0.57 | 0.74 | 0.77 | 0.74 | 1.05 | 0.27 | 0.27 | 0.26 |
| LOI | 0.75 | 0.70 | 0.60 | 0.75 | 0.74 | 0.62 | 0.76 | 0.86 | 0.74 | 0.74 | 1.00 | 1.02 | 0.93 | 1.14 | 1.12 |
| Tot. | 99.42 | 99.03 | 98.81 | 98.88 | 98.98 | 99.27 | 98.76 | 99.04 | 99.07 | 100.63 | 98.97 | 100.00 | 99.32 | 101.92 | 100.08 |
| Mg# | 49 | 46 | 48 | 44 | 46 | 45 | 43 | 45 | 42 | 42 | 42 | 44 | 60 | 60 | 60 |
| C.I.P.W. Norm (wt.%) | | | | | | | | | | | | | | | |
| Q | | | | | | | | | | | | | 2.2 | 6.4 | 7.1 |
| Hy | 11.0 | 10.7 | 8.0 | 4.7 | 18.0 | 11.7 | 5.5 | 11.2 | 12.4 | 17.5 | 14.3 | 16.6 | 20.8 | 19.6 | 19.4 |
| Ol | 4.9 | 6.1 | 7.3 | 11.8 | 0.1 | 4.7 | 10.2 | 5.2 | 4.0 | 0.1 | 2.2 | 2.8 | | | |
| *Trace elements (ppm)* | | | | | | | | | | | | | | | |
| Li | 6.1 | 7.1 | 6.7 | | 8.7 | 5.8 | | | 8.8 | 9.9 | 9.8 | | 6.8 | 7.0 | 9.1 |
| Be | 1.4 | 1.3 | 1.3 | | 1.3 | 1.2 | | | 2.1 | 2.2 | 2.1 | | 1.0 | 1.0 | 0.9 |
| Sc | 17 | 19 | 16 | | 18 | 18 | | | 18 | 18 | 18 | | 18 | 20 | 19 |
| V | 231 | 240 | 230 | | 237 | 225 | | | 171 | 160 | 167 | | 154 | 161 | 165 |
| Cr | 14 | 22 | 14 | | 16 | 19 | | | 1 | 1 | 2 | | 214 | 230 | 221 |
| Co | 44 | 43 | 42 | | 42 | 43 | | | 35 | 33 | 34 | | 39 | 40 | 41 |
| Ni | 55 | 47 | 56 | | 47 | 47 | | | 10 | 8 | 11 | | 140 | 143 | 152 |
| Rb | 10.4 | 12.4 | 15.4 | | 14.8 | 14.3 | | | 21.9 | 22.3 | 21.1 | | 10.6 | 7.1 | 5.0 |
| Sr | 670 | 610 | 675 | | 587 | 609 | | | 556 | 548 | 539 | | 373 | 380 | 392 |
| Y | 25.7 | 30.3 | 25.7 | | 29.8 | 29.3 | | | 42 | 43 | 44 | | 20.4 | 20.5 | 20.3 |
| Zr | 208 | 228 | 207 | | 222 | 220 | | | 363 | 380 | 356 | | 118 | 118 | 120 |
| Nb | 32 | 33 | 32 | | 33 | 33 | | | 47 | 48 | 46 | | 13.6 | 13.6 | 14.0 |
| Cs | 0.17 | 0.27 | 0.45 | | 0.32 | 0.25 | | | 0.32 | 0.30 | 0.35 | | 0.44 | 0.24 | 0.16 |
| Ba | 261 | 306 | 256 | | 296 | 278 | | | 405 | 413 | 396 | | 163 | 146 | 144 |
| La | 24.0 | 25.5 | 24.1 | | 26.3 | 25.5 | | | 41 | 42 | 41 | | 13.7 | 14.2 | 13.4 |
| Ce | 52 | 55 | 52 | | 55 | 53 | | | 88 | 90 | 87 | | 26.9 | 26.7 | 27.4 |
| Pr | 7.1 | 7.4 | 7.1 | | 7.6 | 7.4 | | | 11.6 | 12.0 | 11.6 | | 3.8 | 3.9 | 3.8 |
| Nd | 31 | 33 | 31 | | 33 | 33 | | | 50 | 51 | 50 | | 17.4 | 18.0 | 17.9 |
| Sm | 7.2 | 7.7 | 7.1 | | 7.9 | 7.8 | | | 11.3 | 11.4 | 11.3 | | 4.9 | 4.9 | 5.0 |
| Eu | 2.41 | 2.72 | 2.59 | | 2.77 | 2.83 | | | 3.7 | 3.8 | 3.7 | | 1.84 | 1.79 | 1.90 |

(*continued on next page*)

Table 2 (*continued*)

| | Group I volcanics | | | | | | | | | | | | Group II volcanics | | |
|---|---|---|---|---|---|---|---|---|---|---|---|---|---|---|---|
| Sample | PA-322 | PA-315 | PA-324 | PA-311 | PA-317 | PA-309 | PA-308 | PA-312 | PA-306 | PA-302 | PA-303 | PA-307 | PA-320 | PA-318 | PA-319 |
| Lat. S | 50°24′20″ | 50°19′03″ | 50°32′57″ | 50°18′06″ | 50°18′00″ | 50°17′36″ | 50°19′17″ | 50°18′05″ | 50°19′38″ | 50°20′47″ | 50°20′47″ | 50°19′22″ | 50°24′30″ | 50°23′18″ | 50°23′37″ |
| Long. W | 71°09′41″ | 71°07′33″ | 71°00′26″ | 71°08′00″ | 71°10′29″ | 71°09′37″ | 71°13′07″ | 71°07′50″ | 71°13′22″ | 71°13′20″ | 71°13′20″ | 71°13′16″ | 71°06′35″ | 71°02′22″ | 71°03′03″ |
| Rock | B | B | B | B | B | B | B | B | TB | TB | TB | TB | BA | BA | BA |
| Gd | 6.6 | 7.8 | 6.7 | | 7.6 | 7.6 | | | 10.4 | 10.4 | 10.9 | | 5.2 | 5.3 | 5.1 |
| Tb | 0.92 | 1.04 | 1.01 | | 1.17 | 1.12 | | | 1.53 | 1.61 | 1.59 | | 0.78 | 0.71 | 0.79 |
| Dy | 5.1 | 6.1 | 5.2 | | 6.1 | 5.9 | | | 8.3 | 8.5 | 8.5 | | 4.1 | 4.1 | 4.2 |
| Ho | 0.95 | 1.13 | 0.94 | | 1.12 | 1.10 | | | 1.56 | 1.59 | 1.60 | | 0.74 | 0.75 | 0.77 |
| Er | 2.30 | 2.67 | 2.3 | | 2.65 | 2.63 | | | 3.9 | 4.0 | 4.0 | | 1.81 | 1.79 | 1.83 |
| Tm | 0.33 | 0.38 | 0.30 | | 0.39 | 0.36 | | | 0.53 | 0.56 | 0.56 | | 0.25 | 0.26 | 0.25 |
| Yb | 1.77 | 2.11 | 1.70 | | 2.12 | 2.00 | | | 2.97 | 3.16 | 3.17 | | 1.41 | 1.39 | 1.37 |
| Lu | 0.22 | 0.29 | 0.24 | | 0.28 | 0.27 | | | 0.43 | 0.44 | 0.45 | | 0.19 | 0.18 | 0.19 |
| Hf | 4.9 | 5.5 | 4.9 | | 5.5 | 5.3 | | | 8.3 | 8.7 | 8.2 | | 2.98 | 2.89 | 3.14 |
| Ta | 2.04 | 2.14 | 2.04 | | 2.13 | 2.12 | | | 2.88 | 2.96 | 2.83 | | 0.80 | 0.79 | 0.83 |
| Pb | 1.6 | 2.0 | 1.6 | | 2.4 | 1.8 | | | 3.5 | 1.9 | 4.4 | | 1.5 | 1.5 | 1.4 |
| Th | 2.29 | 2.52 | 2.32 | | 2.80 | 2.42 | | | 4.1 | 4.3 | 4.0 | | 1.53 | 1.48 | 1.49 |
| U | 0.63 | 0.58 | 0.68 | | 0.65 | 0.64 | | | 1.05 | 1.13 | 1.01 | | 0.44 | 0.37 | 0.32 |
| $^{87}Sr/^{86}Sr$ whole rock | | | 0.703525 | | | 0.703704 | | | | | | | 0.703918 | | 0.703908 |
| $^{143}Nd/^{144}Nd$ whole rock | | | 0.512912 | | | 0.512884 | | | | | | | 0.512771 | | 0.512777 |
| $^{87}Sr/^{86}Sr$ plagioclase | | | 0.703569 | | | | | | | | | | | | |
| $^{143}Nd/^{144}Nd$ plagioclase | | | 0.512903 | | | | | | | | | | | | |

B, basalt; TB, trachybasalt; BA, basaltic andesite.

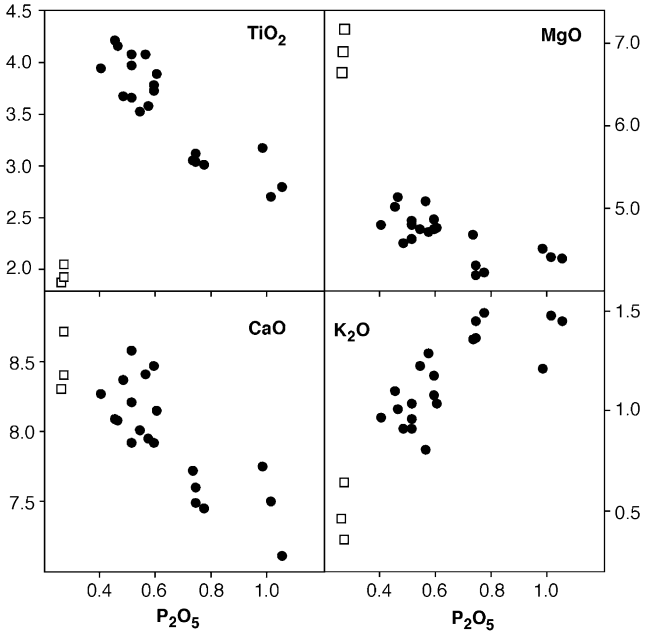


Fig. 7. $TiO_2$, MgO, CaO, $K_2O$ versus $P_2O_5$ (wt.%) variation diagrams for the CAVF rocks. Symbols as in Fig. 5.

characterized by higher radiogenic Sr and lower radiogenic Nd isotope compositions and plot within the field 'B' that encloses the majority of basalts from southern Patagonia.

## 8. Discussion

### *8.1. The CAVF in the frame of Cenozoic southern Patagonia magmatism*

The $^{40}Ar$–$^{39}Ar$ geochronological data we obtained indicate that the volcanic activity in the CAVF occurred during the Late Pliocene in a time interval of approximately 450 ka. Volcanic activity involved the eruption of high-Ti, low-Mg# magmas at 2.9 Ma (Group I lavas), followed by the emission of subordinate basaltic andesites at 2.5 Ma (Group II lavas). Late Pliocene basaltic volcanism is widespread in the Patagonian region south of 46.5°S; volcanics dated 3.6–1.8 Ma have been found, from south to north, in the following volcanic areas: PAVF, Meseta de las Vizcachas, Cerro del Fraile, the mesetas to the north of Río Santa Cruz valley, Meseta del Viento, Meseta Central, Meseta Belgrano, the mesetas north and northeast of the Deseado Massif, and Meseta del Lago Buenos Aires (Charrier et al., 1979; Linares and Gonzalez, 1990; Meglioli, 1992; Gorring, 1997; Mejia et al., 2004). In the area between 46.5°S and 49.5°S, Pliocene-Quaternary volcanism was preceded by the voluminous effusion of lavas, both subalkaline and alkaline, during the Miocene and Oligocene (Baker et al., 1981; Gorring et al., 1997). Although this important phase of magmatism was not known south of 49.5°S, recent geochronological data

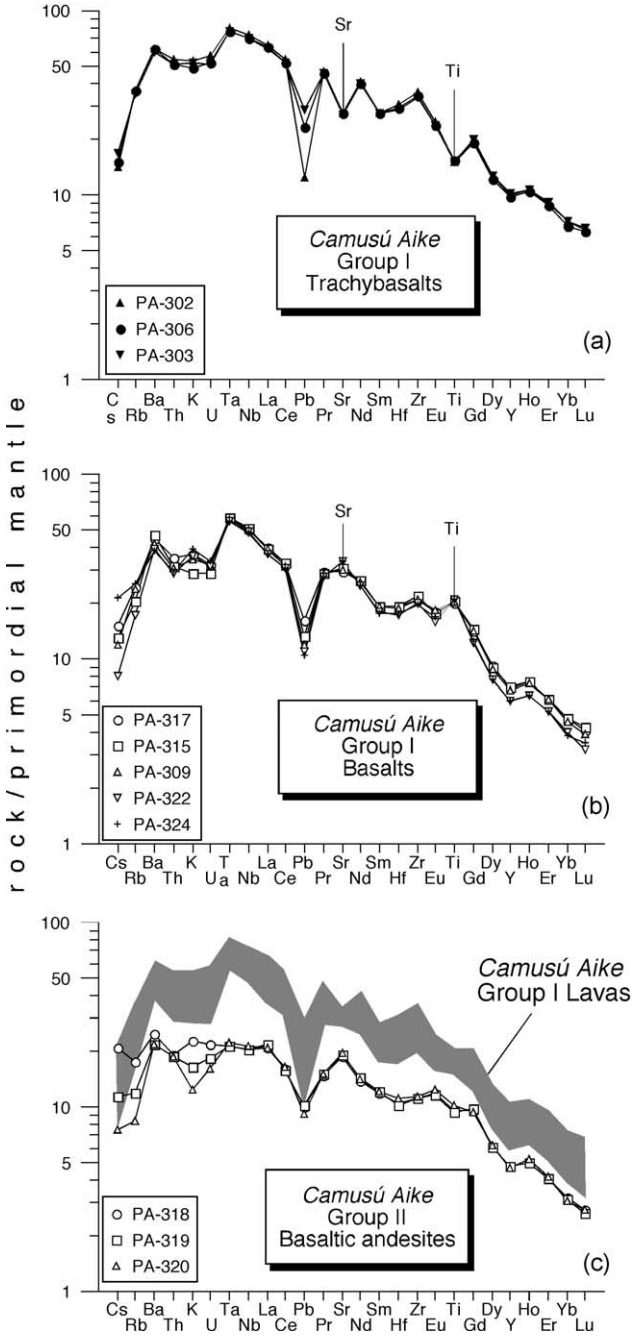


Fig. 8. Primordial mantle-normalized incompatible element patterns for CAVF volcanics. Normalizing values after McDonough and Sun (1995).

indicate that Miocene volcanics were erupted in this section of southern Patagonia in the EGA (D'Orazio et al., 2001) and in the basal sections of the Meseta de las Vizcachas (authors' unpublished data; Mejia et al., 2004). In the latter area, this Middle Miocene phase of volcanism seems volumetrically important.

The two different groups of lavas erupted in the CAVF are reminiscent of the main- and postplateau lavas defined by Gorring et al. (1997) for the Patagonian plateau lavas between 46.5° and 49.5°S. However, in each area of that

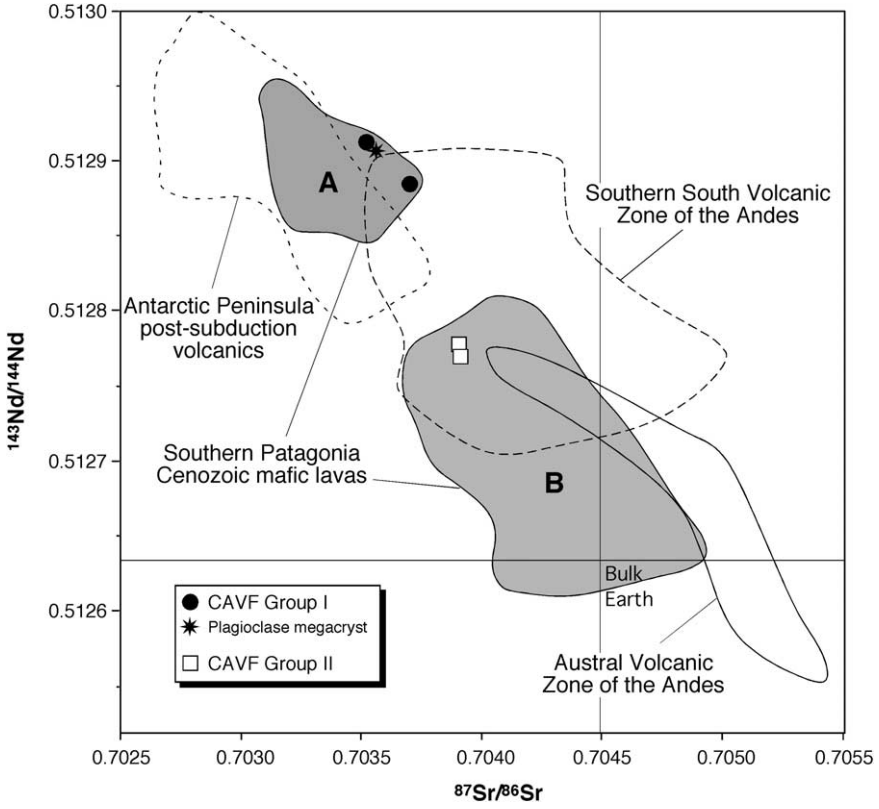


Fig. 9. $^{143}Nd/^{144}Nd$ versus $^{87}Sr/^{86}Sr$ diagram for the CAVF volcanics. Also shown are the fields for Cenozoic postsubduction volcanics from the Antarctic peninsula (Hole et al., 1993, 1995; D'Orazio et al., 1999), the southern Patagonia Cenozoic lavas (Stern et al., 1990; Gorring et al., 1997, 2003; D'Orazio et al., 2000, 2001), and the southern south volcanic zone and austral volcanic zone of the Andes (Hickey-Vargas et al., 1986, 1989; Futa and Stern, 1988; Gerlach et al., 1988; López-Escobar et al., 1993; Stern and Kilian, 1996; D'Orazio et al., 2003 and references therein).

sector of Patagonia, the main-plateau magmatic activity systematically predates by 2–5 Ma the postplateau activity, whereas in the CAVF, the Group II lavas (which may represent the main-plateau lavas) are slightly younger than the Group I lavas (which could represent the postplateau lavas). Moreover, the CAVF Group II lavas were not erupted in large volumes, as usually occurs for main-plateau lavas to the north.

The CAVF is located on that portion of South America east of the segment of the Chile ridge that collided with the Chile trench at approximately 13–14 Ma (Cande and Leslie, 1986). In accordance with the slab window model (Ramos and Kay, 1992; Gorring et al., 1997; D'Orazio et al., 2000), if we assume a convergence rate between the Nazca and South American plates of 9–10 cm $yr^{-1}$ during the past 25 my and a subduction angle of 20–30° (Jarrard, 1986; Cande and Leslie, 1986), the trailing edge of the Nazca plate would have crossed the Camusú Aike area 4–5 my after the ridge-trench collision, or 5–7 my before the eruption of the studied lavas. The time interval between the passage of the trailing edge of the Nazca plate and the eruption of the CAVF magmas was sufficiently long to allow the full development of a slab window. Asthenospheric mantle rising into the space created by the window opening would melt by decompression to become the main source of the CAVF magmas.

### 8.2. Petrogenesis of CAVF magmas

#### 8.2.1. Relationships between Group I and Group II CAVF lavas

The geochemical and isotopic study of the CAVF volcanics clearly suggests two kinds of erupted magmas: Group I basalts and trachybasalts and Group II basaltic andesites. Notwithstanding the strikingly different compositions of these magmas, we explore the possibility that they could be related by crystal fractionation and/or crustal assimilation processes.

Simulations carried out with the thermodynamic codes MELTS/pMELTS (Ghiorso and Sack, 1995; Ghiorso et al., 2002), starting with the composition of the most primitive Group II lava (PA-320), indicate that fractional crystallization at pressures of 10–1 kbar do not drive the residual liquid to compositions that match those of Group I lavas (Fig. 10). The assimilation of Patagonian crust should generate a concurrent increase of $^{87}Sr/^{86}Sr$, $SiO_2$, and LILE and a decrease of $^{143}Nd/^{144}Nd$, Mg#, and compatible trace elements. However, the observed variations are in contrast with those expected for a crustal assimilation process.

In conclusion, the two series of magmas erupted at the CAVF cannot be related by either crystal fractionation at low or high pressures or assimilation of crustal materials.

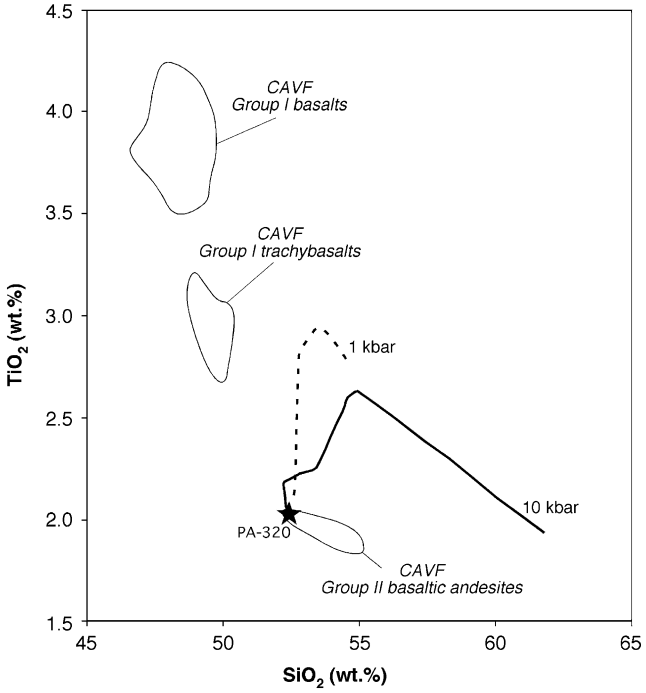


Fig. 10. $TiO_2$ versus $SiO_2$ (wt.%) diagram showing the fields for Group I CAVF basalts and Group II CAVF basaltic andesites. Also plotted are liquid lines of descent for the fractional crystallization of a magma with the bulk composition of sample PA-320. Crystal fractionation simulations were performed using the thermodynamic codes MELTS and pMELTS at pressures of 1 and 10 kbar, respectively (Ghiorso and Sack, 1995; Ghiorso et al., 2002).

*8.2.2. The role of crustal contamination*

The low Mg#s of the Group I CAVF volcanics, coupled with the plagioclase megacrysts hosted in some lavas, indicate the ponding and differentiation of these magmas at shallow levels within the Patagonian continental crust. This condition could have favored the interaction of magmas with crustal materials. However, the Group I volcanics analyzed for Sr–Nd isotopes are characterized by some of the most depleted values of the southern Patagonia magmatic province (Fig. 9). Moreover, the plagioclase megacrysts separated from sample PA-324 were found in (Nd), or close to (Sr), isotope equilibrium with the host rock (Table 2).

Group II lavas are characterized by less differentiated compositions, high $SiO_2$ values, and more enriched Sr–Nd isotopes. In Fig. 9, the two Group II samples plot in that portion of field "B" that is characterized by the highest $^{143}Nd/^{144}Nd$ and lowest $^{87}Sr/^{86}Sr$ ratios. If Group II CAVF magmas acquired their geochemical and isotopic characteristics through upper-crust assimilation processes, the uncontaminated initial magmas should have Sr–Nd isotope compositions similar to those in field 'A.' However, Patagonian lavas in this field are characterized by elevated concentrations of highly incompatible trace elements (Th, Nb, LREE), whereas the Group II lavas have concentrations of these elements below both these magmas and typical continental crust.

In summary, the available geochemical and Sr–Nd isotope data do not support crustal assimilation as a major process in the evolution of the magmas erupted in the CAVF.

*8.2.3. Magmatic evolution of Group I lavas*

As stressed in the previous section, the CAVF lavas of Group I are characterized by a peculiar whole-rock chemistry. They are among the most evolved southern Patagonia lavas in terms of MgO, Ni, and Cr contents but have low contents of incompatible elements, particularly $K_2O$, Rb, Cs, Ta, Nb, Th, U, and LREE. Evidently, the tectonic stress field needed for the stagnation and differentiation of basaltic magmas at shallow levels in the crust did not occur frequently in southern Patagonia during the Cenozoic, as indicated by the dominance of highly primitive lavas.

We simulated the major-element compositions of the CAVF Group I lavas by a crystal fractionation model using the MELTS/pMELTS codes. We hypothesized a two-stage process. In the first fractionation stage, a primitive Patagonian magma stagnates at the base of the crust ($P = 10$ kbar, $\sim 35$ km), segregating an arbitrarily assumed amount of solids of 20 wt.%. In the second stage, the fractionated magma rises into a shallow magma chamber ($P = 1$ kbar, $\sim 3.5$ km) where it fractionates further and approaches the composition of the CAVF Group I basalts and trachybasalts (Fig. 11).

From the available data set of southern Patagonia primitive lavas (i.e. those with Mg# $> 65$), we selected the starting composition for our model from those characterized by a subalkaline affinity (i.e. normative nepheline $= 0$) and a $TiO_2$ content $> 2$ wt.%. These selection criteria were fulfilled only by some lavas from the PAVF (D'Orazio et al., 2000). In Table 3, we report the composition of PA-113, the PAVF lava selected as the starting magma. The fractionated phases in the first stage of the model (from 1320 °C, Liquidus of the starting magma, to 1270 °C), are 20 wt.% of olivine and clinopyroxene in a weight ratio of approximately 1:7. In the second stage of differentiation, the fractionation of a solid assemblage of olivine, spinel (chromite followed by Ti-magnetite), plagioclase, and clinopyroxene, for a total of $\sim 35$ wt.% removed, drives the residual liquid to a composition close to the CAVF basalt. Further fractionation of an additional 11 wt.% of the same phases drives the residual liquid to the composition of the CAVF trachybasalt. The final temperature of 1110 °C in the model is very close to the equilibration temperature of 1080 °C obtained, according to the Fe–Ti oxides geothermometer, for the groundmass of the CAVF Group I basalt PA-324.

The major-element composition of the final liquids obtained with the proposed two-stage model (columns C and E, Table 3) matches the average composition of

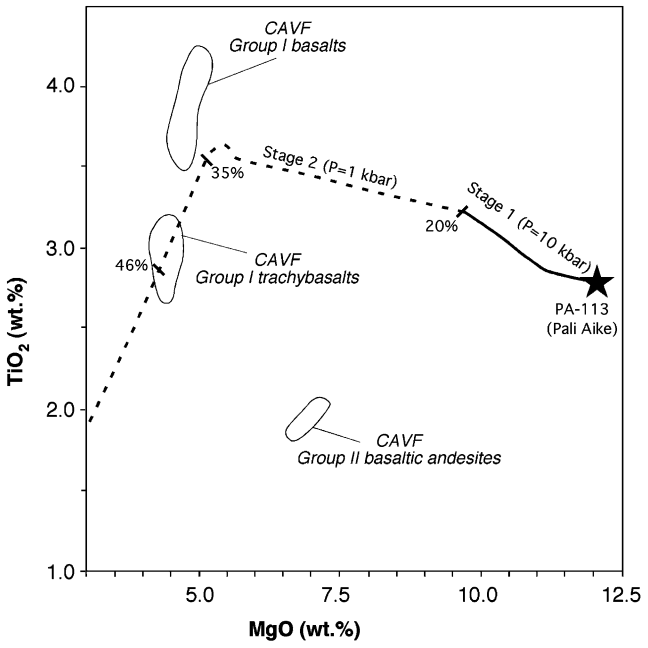


Fig. 11. $TiO_2$ versus MgO (wt.%) diagram showing the fields for the CAVF lavas and the liquid line of descent for the two-stage fractional crystallization of a magma with the bulk composition of PAVF sample PA-113. Stage 1 involves the crystal fractionation of 20 wt.% olivine + clinopyroxene at the base of the crust ($P=10$ kbar), and stage 2 involves the crystal fractionation of a solid assemblage of olivine, plagioclase, clinopyroxene, and spinel (followed by Ti-magnetite) in a shallow magma chamber ($P=1$ kbar). Crystal fractionation simulations were performed using the thermodynamic codes MELTS and pMELTS at pressures of 1 and 10 kbar, respectively. Numbers along the liquid line of descent refer to the wt.% of the fractionated solid.

Table 3
Crystal fractionation simulations carried out with the thermodynamic codes pMELTS/MELTS

| Stage | 1 | | 2 | | | |
|---|---|---|---|---|---|---|
| $P$ (kbars) | 10 | | 1 | | | |
| Melt fraction | 1.00 | 0.805 | 0.652 | | 0.537 | |
| | A | B | C | D | E | F |
| $SiO_2$ (wt.%) | 47.08 | 46.52 | 48.08 | 48.40 | 50.71 | 49.72 |
| $TiO_2$ | 2.78 | 3.22 | 3.55 | 3.85 | 2.86 | 3.01 |
| $Al_2O_3$ | 13.07 | 15.07 | 16.65 | 16.50 | 16.89 | 16.67 |
| $Cr_2O_3$ | 0.06 | 0.08 | 0.00 | 0.00 | 0.00 | 0.00 |
| $Fe_2O_3$ | 1.65 | 1.76 | 2.05 | 4.60 | 1.88 | 4.00 |
| FeO | 9.68 | 10.6 | 10.08 | 8.15 | 8.91 | 8.60 |
| FeO tot | 11.16 | 12.18 | 11.92 | 12.28 | 10.60 | 12.20 |
| MgO | 12.04 | 9.68 | 5.14 | 4.87 | 4.31 | 4.39 |
| CaO | 9.61 | 8.19 | 8.57 | 8.26 | 7.56 | 7.58 |
| $Na_2O$ | 2.58 | 3.11 | 3.70 | 3.49 | 4.24 | 3.72 |
| $K_2O$ | 0.94 | 1.16 | 1.42 | 1.08 | 1.72 | 1.43 |
| $H_2O$ | 0.50 | 0.62 | 0.76 | 0.80 | 0.93 | 0.89 |

A, Starting liquid composition (PAVF sample PA-113; D'Orazio et al., 2000); B, Liquid composition obtained fractionating 2.5 wt.% olivine (avg. composition $Fo_{86.8}$) + 17.0 wt.% clinopyroxene (avg. $Wo_{38}En_{54}Fs_8$) from liquid A. Liquidus $T=1320$ °C, final $T=1270$ °C; C, Liquid composition obtained fractionating 11.6 wt.% olivine (avg. composition $Fo_{81.7}$) + 3.1 wt.% clinopyroxene (avg. $Wo_{53}En_{38}Fs_9$) + 3.5 wt.% plagioclase (avg. $An_{72.9}$) + 0.8 wt.% spinel (chromite + Ti-magnetite) from liquid B. Liquidus $T=1260$ °C, final $T=1125$ °C; D, Average composition of CAVF basalts; E, Liquid composition obtained fractionating at $P=1$ kbar, 12.1 wt.% olivine (avg. composition $Fo_{81.4}$) + 8.8 wt.% clinopyroxene (avg. $Wo_{50}En_{40}Fs_{10}$) + 8.3 wt.% plagioclase (avg. $An_{71.3}$) + 4.3 wt.% spinel (chromite + Ti-magnetite) from liquid B. Liquidus $T=1260$ °C, final $T=1110$ °C; F, Average composition of CAVF trachybasalts.

the CAVF Group I basalts (column D, Table 3) and trachybasalts (column F, Table 3) reasonably well. The chemical component with the largest deviation between calculated and observed values is $K_2O$. However, considering the large uncertainties related to the choice of the starting magma and the assumptions used in the model, we judge the obtained solution to be satisfactory for our purposes.

The incompatible element distribution of the PAVF lavas is similar to those of the CAVF Group I except for higher contents of the most incompatible elements (e.g. Rb, Ba, K, Th, U, Nb, Ta, LREE; Fig. 12). Therefore, we argue that the source of the CAVF Group I magmas was less enriched in highly incompatible elements than was the source of PAVF magmas.

### 8.3. Mantle sources of CAVF magmas

The geochemical and Sr–Nd isotope characteristics of the CAVF Group I lavas provide a typical within-plate signature, very similar to that of the southernmost Patagonia lavas from the PAVF and EGA. Moreover, the reasonably evolved nature of the Group I lavas can be modeled by a polybaric crystal fractionation process, starting from an initial magma whose major-element composition is akin to primitive basalts found in the PAVF. Therefore, we consider these lavas the evolved products of melts derived from the relatively depleted asthenosphere, which then rose through the slab window that had opened below southernmost Patagonia (D'Orazio et al., 2000, 2001).

The nature of the mantle source(s) involved in the genesis of the Group II lavas is more difficult to explain. Although the geochemistry of these lavas is dominated by a within-plate signature, they have a slightly enriched Sr and Nd isotope composition, similar to most Patagonian lavas to the north (Fig. 9), and LREE/HFSE ratios (e.g. La/Nb) that are higher than the typical within-plate values observed for the PAVF, EGA, and CAVF Group I lavas (La/Nb = 0.6–0.8; Fig. 12). Moreover, the LREE/HREE fractionation of Group II lavas is among the lowest of the southern Patagonia region. These geochemical features can be explained if we assume a heterogeneous asthenospheric mantle source or, alternatively, invoke an interaction between the asthenosphere and an enriched mantle component residing in the basal continental lithospheric mantle or the former mantle wedge. However, the existing data indicate that southernmost Patagonia has a homogeneous, isotopically depleted asthenosphere (Stern et al., 1990; D'Orazio et al., 2000, 2001; Gorring

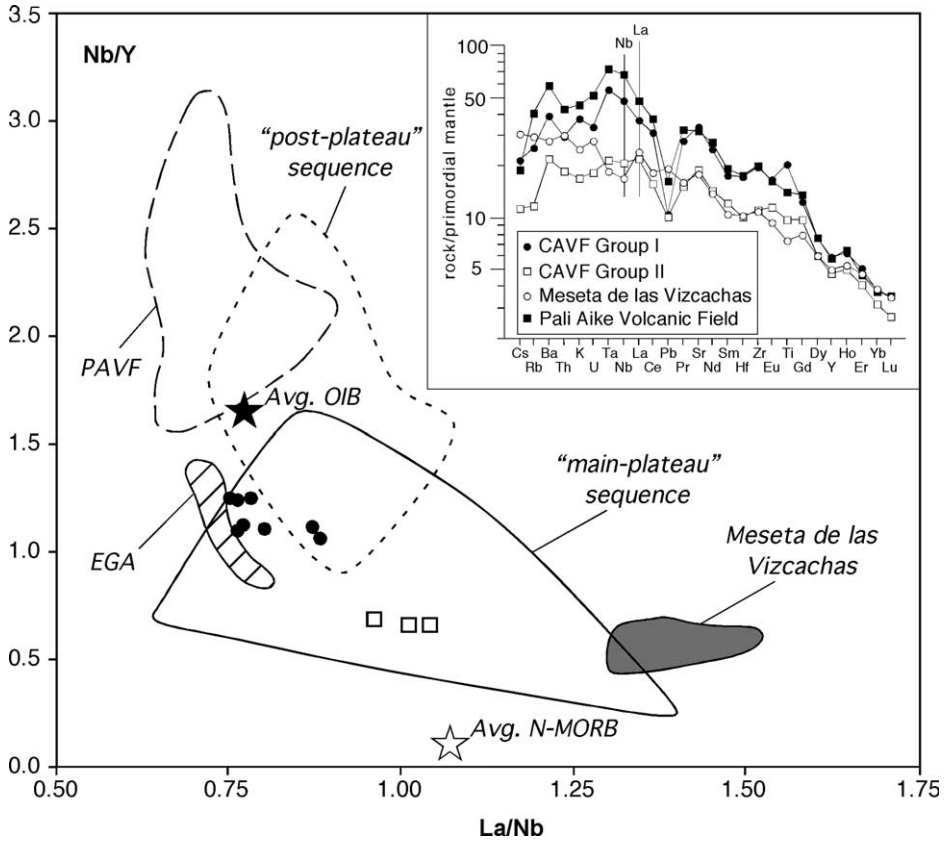


Fig. 12. Nb/Y versus La/Nb diagram for Groups I and II CAVF volcanics. Also plotted are the fields for PAVF (D'Orazio et al., 2000), EGA (D'Orazio et al., 2001), Meseta de las Vizcachas (authors' unpublished data), and main- and postplateau lavas (Gorring et al., 1997). Black and white stars are the average OIB and N-MORB values (Sun and McDonough, 1989), respectively. The inset shows the primordial mantle-normalized incompatible element patterns of four representative samples from CAVF, PAVF, and Meseta de las Vizcachas.

and Kay, 2001) rather than one that is heterogeneous over short distances.

Considering the geological evolution of southern Patagonia in the last 500–600 Ma (age of the stabilization of the mantle lithosphere in this region; Ramos, 1988), two main types of enrichment processes can be envisaged: (1) an asthenosphere melt metasomatism related to either the large-scale Middle Jurassic magmatism associated with the Gondwana break up (e.g. Pankhurst et al., 1998; Féraud et al., 1999) or the Cenozoic Patagonian mafic magmatism (e.g. Stern et al., 1990; Ramos and Kay, 1992) and (2) a fluid/melt mantle metasomatism, associated with the subduction of oceanic plates beneath southern South America since the Cretaceous.

Studies of mantle xenoliths carried by Patagonian volcanics indicates that the continental mantle lithosphere is invariably isotopically depleted but often affected by modal or cryptic recent metasomatism. The nature of the metasomatic agent/process is controversial. Some authors (Gorring and Kay, 2000) invoke a strong carbonatite metasomatism at $<25$ Ma; others (Laurora et al., 2001) suggest that the metasomatic agent was a hydrous fluid or silicate melt, possibly from a subducted slab; still others hypothesize a slab melt component with adakitic affinity for the metasomatism of the Cerro del Fraile mantle xenoliths (Kilian and Stern, 2002). Whatever the nature of the enrichment process, the lithospheric mantle represented by these xenoliths is not a viable isotopic contaminant for the CAVF Group II magmas that have more enriched Sr–Nd isotope compositions. Thus, we argue that the enriched mantle domains are located in a deeper region of the mantle that was not sampled as xenoliths by the uprising magma.

The available geochemical data about Group II lavas—in particular the (LREE+Ba+Th+U)/HFSE ratios slightly above typical within-plate values (Fig. 12)—suggest slab-derived metasomatic components in the source of these magmas. In Fig. 12, we report the Nb/Y versus La/Nb ratios of some volcanics from southern Patagonia. The Nb/Y ratio indicates the degree of partial melting, whereas the La/Nb ratio indicates source heterogeneity, mainly related to subduction-related components. In this diagram, the CAVF Group II lavas fall in the space between the fields for the PAVF, EGA, and CAVF Group I and the field for the lavas from Meseta de las Vizcachas. The latter are characterized by a subduction-related imprint, as shown in the primordial mantle-normalized incompatible element pattern in the inset of Fig. 12.

## 9. Summary and conclusions

The CAVF was active during the Late Pliocene in a backarc setting located approximately 170 km east of the Andean Cordillera axis. Magmas were erupted as lava flows or scoriae and formed a volcanic field of approximately 200 $km^2$. Volcanic rocks can be divided into two basic groups. Group I rocks are ~2.9 Ma basalts and trachybasalts characterized by high-$TiO_2$ contents, low Mg#s, within-plate incompatible element distributions, and depleted Sr–Nd isotope ratios. They appear to be the end product of a polybaric crystal fractionation process that started from typical asthenospheric slab window melts with compositions close to some magmas erupted in the PAVF. Group II rocks are ~2.5 Ma, relatively primitive basaltic andesites characterized by high-$SiO_2$ contents, lower incompatible element contents, higher (LREE, Ba, Th, U)/HFSE ratios, and more enriched Sr–Nd isotope compositions. They also are interpreted as products of slab window magmatism; in this case however, asthenospheric melts suggest a modest contribution from an enriched reservoir. In consideration of the long subduction history of the Pacific margin of South America and the geochemical anomalies (e.g. slightly high LREE, Ba, Th, U/HFSE ratios) of the Group II lavas, we believe that the enriched component likely is represented by materials derived from prior subduction of the Nazca plate.

The study of the volcanic rocks that form the CAVF has revealed a significant geochemical variability in magmas erupted in a relatively small area and a short time interval. In particular, in the CAVF, moderately differentiated lavas that rarely are found in the other southern Patagonia Cenozoic volcanic formations occur. These features are primarily related to the geochemical heterogeneity of the mantle source below the CAVF and the modalities of magma ascent (the latter also is related to the local stress field). The factors that control the origin, chemical evolution, and geodynamic significance of the Cenozoic mafic magmatism of southern Patagonia will be fully evaluated in additional investigations in which we integrate petrological, geochemical, and geochronological data with geophysical and structural data.

Table A1
$^{40}Ar$–$^{39}Ar$ laser step-heating analyses. Argon data $\times 10^{-15}$ moles

| No. | $^{36}Ar_{(atm)}$ | $^{37}Ar_{(Ca)}$ | $^{38}Ar_{(Cl)}$ | $^{39}Ar_{(K)}$ | $^{40}Ar_{(Tot)}$ | Age (Ma) | $\pm 2\sigma$ | $^{40}Ar^{*}$ % | $^{39}Ar_{(K)}$ % | Ca/K | $\pm 2\sigma$ |
|---|---|---|---|---|---|---|---|---|---|---|---|
| Sample PA-309, $J = 0.0003622 \pm 0.0000011$ | | | | | | | | | | | |
| 1 | 0.09389 | 0.1671 | 0.01768 | 0.3195 | 28.533 | 1.6 | 2.3 | 2.8 | 2.8 | 0.99 | 0.09 |
| 2 | 0.1948 | 1.687 | 0.04983 | 1.447 | 63.457 | 2.66 | 0.41 | 9.3 | 12.7 | 2.20 | 0.13 |
| 3 | 0.1380 | 2.612 | 0.04568 | 1.765 | 48.281 | 2.78 | 0.30 | 15.6 | 15.5 | 2.79 | 0.17 |
| 4 | 0.07726 | 2.720 | 0.02685 | 1.676 | 30.128 | 2.84 | 0.24 | 24.2 | 14.7 | 3.06 | 0.18 |
| 5 | 0.04332 | 3.268 | 0.01417 | 1.797 | 20.920 | 2.95 | 0.14 | 38.8 | 15.7 | 3.43 | 0.20 |
| 6 | 0.02742 | 4.256 | 0.00732 | 2.003 | 17.332 | 3.01 | 0.07 | 53.2 | 17.5 | 4.01 | 0.24 |
| 7 | 0.03455 | 4.671 | 0.00538 | 1.548 | 17.033 | 2.88 | 0.11 | 40.0 | 13.6 | 5.69 | 0.34 |
| 8 | 0.04094 | 7.147 | 0.00367 | 0.4269 | 13.937 | 2.81 | 0.62 | 13.2 | 3.7 | 31.6 | 1.9 |
| 9 | 0.06277 | 8.260 | 0.00343 | 0.4338 | 20.487 | 2.92 | 0.73 | 9.5 | 3.8 | 35.9 | 2.2 |
| Total fusion | | | | | | 2.83 | 0.11 | | | | |
| Sample PA-320, $J = 0.0003631 \pm 0.0000011$ | | | | | | | | | | | |
| 1 | 0.06425 | 0.4508 | 0.06839 | 0.62656 | 21.272 | 2.39 | 0.61 | 10.7 | 7.8 | 1.36 | 0.10 |
| 2 | 0.10575 | 1.861 | 0.08856 | 1.86091 | 38.411 | 2.52 | 0.18 | 18.6 | 23.1 | 1.89 | 0.12 |
| 3 | 0.06385 | 2.305 | 0.06066 | 1.54081 | 25.266 | 2.72 | 0.19 | 25.3 | 19.1 | 2.82 | 0.17 |
| 4 | 0.04098 | 2.871 | 0.04016 | 1.16351 | 16.462 | 2.45 | 0.18 | 26.4 | 14.4 | 4.66 | 0.28 |
| 5 | 0.02975 | 4.545 | 0.03428 | 1.04270 | 12.658 | 2.43 | 0.14 | 30.5 | 12.9 | 8.23 | 0.49 |
| 6 | 0.01476 | 4.889 | 0.02254 | 0.64360 | 6.798 | 2.48 | 0.24 | 35.8 | 8.0 | 14.33 | 0.85 |
| 7 | 0.01297 | 10.511 | 0.01858 | 0.45640 | 5.714 | 2.70 | 0.34 | 32.9 | 5.7 | 43.5 | 2.6 |
| 8 | 0.01297 | 17.499 | 0.02798 | 0.43265 | 5.464 | 2.47 | 0.53 | 29.8 | 5.4 | 76.3 | 4.6 |
| 9 | 0.00560 | 8.219 | 0.01565 | 0.29265 | 2.682 | 2.30 | 0.53 | 38.3 | 3.6 | 53.0 | 3.3 |
| Total fusion | | | | | | 2.52 | 0.09 | | | | |
| Sample PA-324, $J = 0.0003636 \pm 0.0000011$ | | | | | | | | | | | |
| 1 | 0.04144 | 0.4978 | 0.04186 | 0.6564 | 15.423 | 3.17 | 0.35 | 20.6 | 4.1 | 1.43 | 0.10 |
| 2 | 0.10783 | 3.965 | 0.16068 | 3.307 | 46.183 | 2.84 | 0.17 | 31.0 | 20.6 | 2.26 | 0.15 |
| 3 | 0.04610 | 5.179 | 0.07980 | 2.569 | 24.929 | 2.89 | 0.08 | 45.3 | 16.0 | 3.80 | 0.25 |
| 4 | 0.01979 | 5.321 | 0.02887 | 2.066 | 15.089 | 2.93 | 0.09 | 61.2 | 12.8 | 4.86 | 0.32 |
| 5 | 0.01228 | 5.686 | 0.01771 | 2.202 | 13.536 | 2.95 | 0.10 | 73.1 | 13.7 | 4.87 | 0.32 |
| 6 | 0.01035 | 4.730 | 0.01847 | 1.897 | 11.464 | 2.90 | 0.09 | 73.2 | 11.8 | 4.70 | 0.31 |
| 7 | 0.01284 | 5.031 | 0.01895 | 1.280 | 8.858 | 2.59 | 0.18 | 57.1 | 8.0 | 7.42 | 0.49 |
| 8 | 0.02183 | 11.074 | 0.02985 | 1.526 | 11.807 | 2.30 | 0.15 | 45.3 | 9.5 | 13.69 | 0.88 |
| 9 | 0.00772 | 5.424 | 0.00678 | 0.5769 | 4.571 | 2.60 | 0.20 | 50.0 | 3.6 | 17.7 | 1.1 |
| Total fusion | | | | | | 2.82 | 0.05 | | | | |

## Acknowledgements

The authors thank David Scott Westerman for a critical reading of the manuscript and Marco Bertoli and Marco Tamponi for the XRF analyses. They thank Stella Page and an anonymous referee for their constructive reviews and Victor Ramos for his editorial assistance. The authors are grateful to Federigo and Maria Laura Mau at the Estancia El Refugio for their kind hospitality. This research was supported by MIUR-ITALY and the Italian National Antarctic Research Program (PNRA).

## Appendix A

Table A1

## References

Baker, P.E., Rea, W.J., Skarmeta, J., Caminos, R., Rex, D.C., 1981. Igneous history of the Andean cordillera and Patagonian plateau around latitude 46°S. Philosophical Transactions of the Royal Society of London A303, 105–149.

Baksi, A.K., Archibald, D.A., Farrar, E., 1996. Intercalibration of $^{40}Ar^{39}/Ar$ dating. Chemical Geology 129, 307–324.

Bence, A.E., Albee, A.L., 1968. Empirical correction factors for the electron microanalyses of silicates and oxides. Journal of Geology 76, 382–483.

Biddle, K.T., Uliana, M.A., Mitchum, R.M., Fitzgerald, M.G., Wright, R.C., 1986. The stratigraphic and structural evolution of the central and eastern Magallanes basin, southern South America. In: Allen, P.A., Homewood, P. (Eds.), Foreland Basins, vol. 8: International Association of Sedimentologists Special Publication, pp. 41–61.

Cande, S.C., Leslie, R.B., 1986. Late Cenozoic tectonics of the Southern Chile Trench. Journal of Geophysical Research 91, 471–496.

Charrier, R., Linares, E., Niemeyer, H., Skarmeta, J., 1979. K–Ar ages of basalt flows of the Meseta Buenos Aires in southern Chile and their relation to the southeast Pacific triple junction. Geology 7, 436–439.

Coutand, I., Diraison, M., Cobbold, P.R., Gapais, D., Rossello, E.A., Miller, M., 1999. Structure and kinematics of a foothills transect. Lago Viedma, southern Andes. Journal of South American Earth Sciences 12, 1–15.

Dalziel, I.W.D., 1981. Back-arc extension in the southern Andes: A review and critical reappraisal. Philosophical Transactions of the Royal Society of London 300, 319–335.

DeMets, C., Gordon, R.G., Argus, D.F., Stein, S., 1994. Effect of recent revisions to the geomagnetic reversal time scale on estimate of current plate motions. Geophysical Research Letters 21, 2191–2194.

Diraison, M., Coppold, P.R., Gapais, D., Rossello, E.A., 1997. Magellan Strait: Part of a Neogene rift system. Geology 25, 703–706.

D'Orazio, M., Gonzalez-Ferrán, O., Innocenti, F., Mazzarini, F., Mazzuoli, R., Tonarini, S., Adorni-Braccesi, A., 1999. Alkaline basaltic volcanism in the Weddell Sea side of the northernmost Antarctic Peninsula: Sr–Nd isotope and trace-element characteristics. 8th International Symposium on Antartic Earth Sciences, Wellington, Abstract volume, 92 1999;.

D'Orazio, M., Agostini, S., Mazzarini, F., Innocenti, F., Manetti, P., Haller, M., Lahsen, A., 2000. The Pali Aike Volcanic Field. Patagonia: Slab-window magmatism near the tip of South America. Tectonophysics 321, 407–427.

D'Orazio, M., Agostini, S., Innocenti, F., Haller, M.J., Manetti, P., Mazzarini, F., 2001. Slab window-related magmatism from southernmost South America: The Late Miocene mafic volcanics from the Estancia Glencross area (~52°S Argentina-Chile). Lithos 57, 67–89.

D'Orazio, M., Innocenti, F., Manetti, P., Tamponi, M., Tonarini, S., González-Ferrán, O., Lahsen, A., Omarini, R., 2003. The Quaternary calc-alkaline volcanism of the Patagonian Andes close to the Chile Triple Junction: Geochemistry and petrogenesis of volcanic rocks from the Cay and Maca volcanoes (~45°S Chile). Journal of South American Earth Sciences 16, 219–242.

Féraud, G., Alric, V., Fornari, M., Bertrand, H., Haller, M., 1999. $^{40}Ar/^{39}Ar$ dating of the Jurassic volcanic province of Patagonia: Migrating magmatism related to Gondwana break-up and subduction. Earth and Planetary Science Letters 172, 83–96.

Futa, K., Stern, C.R., 1988. Sr and Nd isotopic and trace element composition of Quaternary volcanic centers of southern Andes. Earth and Planetary Science Letters 88, 253–263.

Gerlach, D.C., Frey, F.A., Moreno-Roa, H., López-Escobar, L., 1988. Recent volcanism in the Puyehue-Cordon Caulle region. Southern Andes, Chile (40.5°S): Petrogenesis of evolved lavas. Journal of Petrology 29, 333–382.

Ghiorso, M.S., Sack, R.O., 1991. Fe–Ti oxide geothermometry. Thermodynamic formulation and the estimation of intensive variables in silicic magmas. Contributions to Mineralogy and Petrology 108, 485–510.

Ghiorso, M.S., Sack, R.O., 1995. Chemical mass transfer in magmatic processes. IV. A revised and internally consistent thermodynamic model for the interpolation and extrapolation of liquid–solid equilibria in magmatic systems at elevated temperatures and pressures. Contributions to Mineralogy and Petrology 119, 197–212.

Ghiorso, M.S., Hirschmann, M.M., Reiners, P.W., Kress III., V.C., 2002. The pMELTS: A revision of MELTS aimed at improving calculation of phase relations and major element partitioning involved in partial melting of the mantle at pressures up to 3 GPa. Geochemistry, Geophysics, Geosystems 3. 101029/2001GC000217.

Gorring, M.L., 1997. Mantle processes associated with ridge-trench collision: Evidence from plateau lavas and xenoliths from Southern Patagonia. PhD Dissertation. Cornell University, Ithaca, NY, USA.

Gorring, M.L., Kay, S.M., 2000. Carbonatite metasomatized peridotite xenoliths from southern Patagonia: Implications for lithospheric processes and Neogene plateau magmatism. Contributions to Mineralogy and Petrology 140, 55–72.

Gorring, M.L., Kay, S.M., 2001. Mantle processes and sources of Neogene slab window magmas from southern Patagonia, Argentina. Journal of Petrology 42, 1067–1094.

Gorring, M.L., Kay, S.M., Zeitler, P.K., Ramos, V.A., Rubiolo, D., Fernandez, M.I., Panza, J.L., 1997. Neogene Patagonian plateau lavas: Continental magmas associated with ridge collision at the Chile Triple Junction. Tectonics 16, 1–17.

Gorring, M.L., Singer, B., Gowers, J., Kay, S.M., 2003. Plio-Pleistocene basalts from the Meseta del Lago Buenos Aires, Argentina: Evidence for asthenosphere-lithosphere interactions during slab window magmatism. Chemical Geology 193, 215–235.

Hervé, F., Davidson, J., Mpodozis, E., Covacevich, E.V., 1981. The late Palaezoic in Chile: Stratigraphy, structure and possible tectonic framework. Annais Acad. Brasil. Ciencias 53, 361–373.

Hickey-Vargas, R., Frey, F.A., Gerlach, D., 1986. Multiple sources for basaltic arc rocks from the Southern Volcanic Zone of the Andes (34–41°S): Trace element and isotopic evidence for contributions from subducted oceanic crust, mantle, and continental crust. Journal of Geophysical Research 91 (B6), 5963–5983.

Hickey-Vargas, R., Moreno-Roa, H., López-Escobar, L., Frey, F.A., 1989. Geochemical variations in Andean basaltic and silicic lavas from the Villarrica–Lanin volcanic chain (39.5°S): An evaluation of source heterogeneity, fractional crystallization and crustal assimilation. Contributions to Mineralogy and Petrology 103, 361–386.

Hole, M.J., Kempton, P.D., Millar, I.L., 1993. Trace-element and isotopic characteristics of small-degree melts of the asthenosphere: Evidence from the alkalic basalts of the Antarctic Peninsula. Chemical Geology 109, 51–68.

Hole, M.J., Saunders, A.D., Rogers, G., Sykes, M.A., 1995. The relationship between alkaline magmatism, lithospheric extension and slab window formation along continental destructive plate margins. In: Smellie, J.L. (Ed.), Volcanism Associated with Extension at Consuming Plate Margins. Geological Society Special Publications, vol. 81, pp. 265–285.

Irvine, T.N., Baragar, W.R.A., 1971. A guide to the chemical classification of the common volcanic rocks. Canadian Journal of Earth Sciences 8, 523–548.

Ivins, E.R., James, T.S., 1999. Simple models for late Holocene and present-day Patagonian glacier fluctuations and predictions of a geodetically detectable isostatic response. Geophysical Journal International 138, 601–624.

Jarrard, R.D., 1986. Relations among subduction parameters. Reviews of Geophysics 24, 217–284.

Kilian, R., Stern, C.R., 2002. Constraints on the interaction between slab melts and the mantle wedge from adakitic glass in peridotite xenoliths. European Journal of Mineralogy 14, 25–36.

Kraemer, P.E., 1998. Structure of the Patagonian Andes: regional balanced cross section at 50°S Argentina. International Geology Review 40, 896–915.

Kraemer, P.E., Introcaso, A., Robles, A., 1996. Perfil geológico-gravimétrico regional a los 50°20′ Latitud Sur. Estructura crustal y acortamiento Andino. Cuenca Austral y Cordillera Patagónica. In: XIII Congreso Geológico Argentino y III Congreso de Exploración de Hidrocarburos, Actas II, 423–432.

Laurora, A., Mazzucchelli, M., Rivalenti, G., Vannucci, R., Zanetti, A., Barbieri, M.A., Cingolani, C.A., 2001. Metasomatism and melting in carbonated peridotite xenoliths from the mantle wedge: The Gobernador Gregores case (Southern Patagonia). Journal of Petrology 42, 69–87.

Linares, E., Gonzalez, R., 1990. Catálogo de edades radimétricas de la República Argentina: 1957–1987, Publicaciones Especiales de la Asociación Geológica Argentina, Serie B, vol. 19 1990. 628pp.

López-Escobar, L., Kilian, R., Kempton, P., Tagiri, M., 1993. Petrography and geochemistry of Quaternary rocks from the Southern Volcanic Zone of the Andes between 41°30′ and 46°00′S Chile. Revista Geológica de Chile 20, 33–55.

McDonough, W.F., Sun, S.S., 1995. The composition of the Earth. Chemical Geology 120, 223–253.

Meglioli, A., 1992. Glacial geology and geochronology of southernmost Patagonia and Tierra del Fuego, Argentina and Chile. PhD dissertation. Leigh University, Bethlehem, PA, USA.

Mejia, V., Opdyke, N.D., Vilas, J.F., Singer, B.S., Stoner, J.S., 2004. Plio-Pleistocene time-averaged field in southern Patagonia recorded in lava flows. Geochemistry, Geophysics, Geosystems 5. 101029/2003GC000633.

Pankhurst, R.J., Leat, P.T., Sruoga, P., Rapela, C.W., Márquez, M., Storey, B.C., Riley, T.R., 1998. The Chon Aike province of Patagonia and related rocks in west Antarctica: A silicic large igneous province. Journal of Volcanology and Geothermal Research 81, 113–136.

Ramos, V.A., 1988. Late Proterozoic–Early Paleozoic of South America—A collisional history. Episodes 11, 168–174.

Ramos, V.A., 1989. Andean foothills structure in northern Magallanes basin, Argentina. American Association of Petroleum Geologists Bulletin 73, 887–903.

Ramos, V.A., Kay, S.M., 1992. Southern Patagonian plateau basalts and deformation: Backarc testimony of ridge collisions. Tectonophysics 205, 261–282.

Skewes, M.A., Stern, C.R., 1979. Petrology and geochemistry of alkali basalts and ultramafic inclusions from the Pali-Aike volcanic field in southern Chile and the origin of the Patagonian plateau lavas. Journal of Volcanology and Geothermal Research 6, 3–25.

Stern, C.R., Kilian, R., 1996. Role of the subducted slab, mantle wedge and continental crust in the generation of adakites from the Andean Austral Volcanic Zone. Contributions to Mineralogy and Petrology 123, 263–281.

Stern, C.R., Frey, F.A., Futa, K., Zartman, R.E., Peng, Z., Kyser, T.K., 1990. Trace-element and Sr, Nd, Pb and O isotopic composition of Pliocene and Quaternary alkali basalt of the Patagonian Plateau lavas of southernmost South America. Contributions to Mineralogy and Petrology 104, 294–308.

Strelin, J.A., Re, G., Keller, R., Malagnino, E., 1999. New evidence concerning the Plio-Pleistocene landscape evolution of southern Santa Cruz region. Journal of South American Earth Sciences 12, 333–341.

Sun, S.S., McDonough, W.F., 1989. Chemical and isotopic systematics of oceanic basalts; Implications for mantle composition and processes. In: Saunders, A.D., Norry, M.J. (Eds.), Magmatism in the Ocean Basins Geological Society Special Publication, vol. 42, pp. 313–345.

Winslow, M.A., 1982. The structural evolution of the Magallanes Basin and neotectonics in the southernmost Andes. In: Craddock, C. (Ed.), Antarctic Geoscience, University of Wisconsin, Madison, pp. 143–154.